Reviews in Mineralogy & Geochemistry
Vol. 63, pp. 399-426, 2006

Neutron Diffraction Texture Analysis

Hans-Rudolf Wenk

Department of Earth and Planetary Science
University of California
Berkeley, California, 94720, U.S.A.
e-mail: wenk@berkeley.edu

INTRODUCTION

An intrinsic property of polycrystalline materials is the orientation distribution of crystallites. In some cases this distribution is random, yet often there is preferred orientation of crystallites relative to macroscopic axes that may have been attained during a deformation process. Many rocks—metamorphic, igneous as well as sedimentary—display non-random orientation distributions that are the cause for anisotropy of macroscopic physical properties. Interpretation of textures in materials has to rely on a quantitative description of orientation characteristics. Two types of preferred orientations need to be distinguished: The *shape preferred orientation* (or often abbreviated SPO) describes the orientation of grains with anisotropic shape. The *lattice preferred orientation* (LPO) or "texture" refers to the orientation of the crystal lattice. (LPO is an unfortunate term since the lattice does not always uniquely describe the crystal orientation, as in the trigonal mineral quartz with a hexagonal unit cell. "Crystallographic preferred orientation," CPO, would be more appropriate). Shape and crystal orientation can be correlated, such as in sheet silicates with a flaky morphology in schists, or fibers in fiber reinforced ceramics. In other cases they are not. In a rolled cubic metal or a plastically deformed quartzite, the grain shape depends on the deformation and is not directly related to the crystallography.

Many methods have been used to determine preferred orientation. Geologists have applied extensively the petrographic microscope equipped with a Universal stage to measure the orientation of morphological and optical directions in individual grains (e.g., Wahlstrom 1979; Wenk 1985). More recently electron diffraction, both with transmission (TEM) and scanning electron microscopes (SEM) have been used to measure orientation of crystals (e.g., Schwarzer and Weiland 1988; Randle and Engel 2000). In this case, the location of a grain can be determined, which permits to correlate microstructures, neighbor relations and texture. Also from individual orientation measurements the orientation distribution can be determined unambiguously. Grain statistics are generally limited to at best a few thousand grains and generally much less, even if many spots are recorded on a polycrystalline sample.

Other diffraction techniques rely on averages of diffraction signals over a polycrystalline sample. In this case spatial information is lost and in addition some ambiguity is introduced about the orientation distribution because normal diffraction effects are always centrosymmetric (Friedel's law) but an orientation relation is not (Matthies 1979). With averaging diffraction techniques statistics are highly improved and crystal orientations are weighted according to grain size.

In this context neutron diffraction plays an important role: For most materials, absorption is negligible compared to X-rays (Fig. 1). Large samples, 1-10 cm in diameter, of roughly spherical shape can be measured. Because the diffraction signal averages over large volumes rather than surfaces grain statistics are even better than with conventional X-rays. Figure 2 compares (0001) pole figures for quartz, one measured with the Universal stage and the other

1529-6466/06/0063-0015$05.00 DOI: 10.2138/rmg.2006.63.15

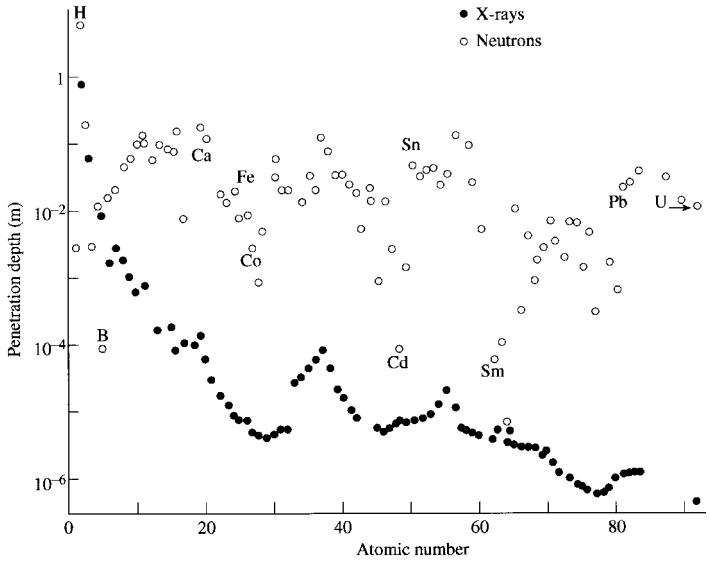

Figure 1. Absorption of neutrons and X-rays. The penetration depth corresponds to the thickness when the intensity has been reduced to 40%. Wavelength is 0.14 nm.

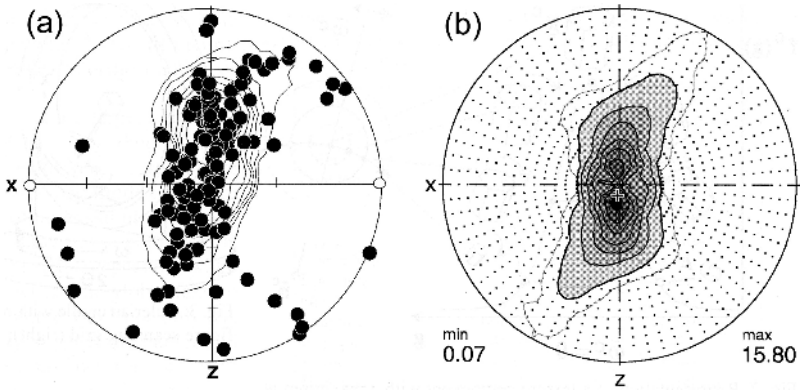

Figure 2. (0001) Pole figures of quartzite measured (a) on one hundred grains with a Universal stage petrographic microscope and (b) a neutron diffractometer with monochromatic radiation, averaging over approximately one million grains (Ghildiyal et al. 1999).

averaged over a million grains by neutron diffraction (Ghildiyal et al. 1999). The limited statistics of Universal stage measurements is obvious. Furthermore for quartz only *c*-axes can be measured with the Universal stage, whereas other crystallographic directions may be just as important to assess deformation characteristics. Figure 3 illustrates similar statistical limitations for calcite marble where pole figures were measured with an X-ray pole figure goniometer in reflection geometry on the surface of a slab (Fig. 3a) and by neutron diffraction on a sample cube (Fig. 3b) (Wenk et al. 1984). The X-ray pole figure shows an irregular pattern, whereas the neutron pole figure displays a symmetrical distribution, representative of the bulk orientation features of the sample. The low absorption has other advantages: Intensity corrections are generally unnecessary and environmental stages (heating, cooling,

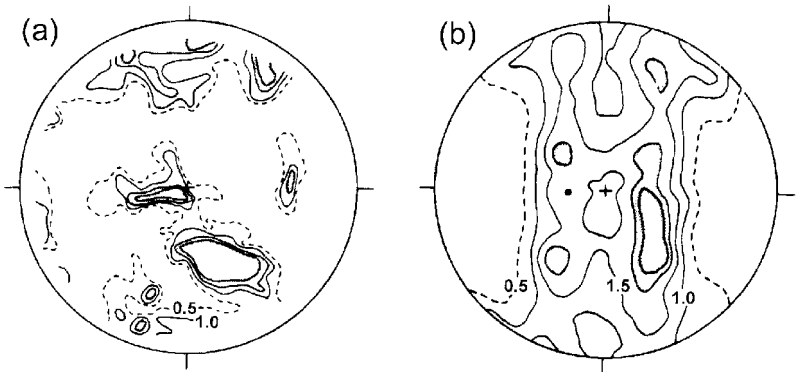

Figure 3. Comparison of (0006) pole figures of calcite for experimentally deformed marble. (a) Measured by X-ray diffraction in reflection geometry. (b) Measured by monochromatic neutron radiation in Jülich (Wenk et al. 1984). Equal area projection.

straining) can be used for *in situ* observation of texture changes. Neutron diffraction was first applied to textures in 1953 by Brockhouse to investigate magnetic structures, though rather unsuccessfully. Yet, during the last twenty years, neutron texture analysis has become firmly established in earth and materials science and has emerged as a favorite technique for many applications. This Chapter will describe the various experimental techniques, survey methods of quantitative data analysis and illustrate neutron texture analysis with examples.

Concepts of texture analysis, including texture representation, experimental techniques and interpretation, have been reviewed in books (e.g., Wenk 1985; Kocks et al. 2000). For earlier reviews of neutron diffraction texture analysis see also Brokmeier (1997, 1999), Feldmann (1989), Schaefer (2002) and Wenk (1994). For texture representations this Chapter will only use pole figures that represent the directional distribution of lattice plane normals {*hkl*} relative to sample coordinates. All pole figures shown use equal area projection of the orientation sphere and display pole densities in multiples of a random distribution (m.r.d.). The integral over a pole figure is 1 m.r.d.

EXPERIMENTAL TECHNIQUES

Neutron diffraction texture analysis relies on Bragg's law that stipulates that neutron waves *reflect* on lattice planes if the condition $2d_{hkl} \sin\theta = \lambda$ is satisfied. In a polycrystalline sample a detector at a particular orientation relative to the incident neutron beam only records signals from lattice planes that satisfy the reflection condition. In a textured sample the overall signal intensity changes if the sample is rotated relative to the detector and, if several detectors are available, each detector records different intensities and differently oriented crystals. From these intensity variations for different lattice planes *hkl* the orientation distribution can be obtained.

For X-ray techniques, whether in reflection or transmission geometry, the incident beam must not leave the specimen during rotations for a straightforward interpretation of intensity variations and proper volume/absorption/defocusing corrections need to be applied during data analysis. By contrast, for neutrons it is advantageous if the specimen does not leave the beam during rotations, so that the same volume is investigated at all times.

The elastic scattering of thermal neutrons by a crystal consists of two components, nuclear and magnetic scattering (see Parise 2006, this volume). *Nuclear scattering* is due to interactions between the neutron and the atomic nuclei and yields diffraction effects with equivalent

information as X-ray scattering on electrons, but magnitudes of the scattering lengths are different and therefore diffraction peaks have different relative intensities. With neutrons signals from light elements are of similar magnitude as those from heavy ones. Also different isotopes can be distinguished. Scattering amplitudes of X-rays decrease with *d*-spacing, whereas those of neutrons do not. This improves the capability to measure low *d*-spacing reflections but their intensity is still lower because of thermal vibration and Lorentz polarization effects. *Magnetic scattering*, due to a dipole interaction between the magnetic moments of nucleus and shell electrons, is weaker (Harrison 2006, this volume). In materials with magnetic elements (e.g., Mn, Fe) peaks may occur in the diffraction pattern that are solely due to magnetic scattering and with those one can measure magnetic pole figures. They do display preferred orientation of magnetic dipoles in component crystals. If no magnetic superstructures are present, the magnetic contribution is, with presently available instrumentation, very difficult to separate from the nuclear scattering. Some examples will be shown later in this chapter.

Neutron diffraction texture studies are done either at reactors with a constant flux of thermal neutrons, or with pulsed neutrons at spallation sources. The wavelength distribution of moderated thermal neutrons is a broad spectrum with a peak at 1–2 Å (Vogel and Priesmeyer 2006, this volume). The low absorption and high penetration of neutrons relative to X-rays was mentioned. This is an expression of the weak interaction of neutrons with matter, which has the disadvantage that scattering is weak and long counting times are required.

A conventional neutron texture experiment at a reactor source uses monochromatic radiation produced with single crystal monochromators. A goniometer rotates the sample to explore the entire orientation range, analogous to an X-ray pole figure goniometer. Such texture measurements are routinely conducted at Chalk River (Canada), Geesthacht (Germany), LLB (France) and NIST (USA). To improve counting efficiency *position-sensitive detectors* have been applied that record a 2θ spectrum with many peaks simultaneously. Examples of such facilities are at ILL (instruments D1B and D20) and Jülich (Julios). With the advent of pulsed neutron sources it has become popular to use *polychromatic* neutrons and detectors that can identify the energy of neutrons by measuring the time of flight (TOF). Dedicated TOF diffractometers for texture research are at JINR, Dubna (SKAT), IPNS (GPPD) and LANSCE (HIPPO).

Monochromatic neutrons

A conventional texture experiment uses monochromatic radiation. With a Cu (111) or graphite (0002) monochromator wavelengths $\lambda = 1.289$ Å and $\lambda = 2.522$ Å are often selected. The detector is aligned relative to the incident beam at the angle 2θ for a selected lattice plane *hkl* to satisfy Bragg's law. The intensities are measured in different sample directions by rotating the sample around two axes with a goniometer (e.g., ϕ and χ), to cover the entire orientation range, often in $5° \times 5°$ increments (Fig. 4). Intensities are directly proportional to pole densities. This method is analogous to that for an X-ray pole figure goniometer but with the advantage that defocusing corrections are not necessary. Figure 5 shows a calcite (0006) pole figure of experimentally deformed limestone that was measured at Geesthacht with this method.

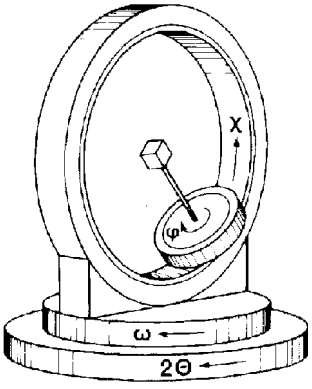

Figure 4. Eulerian cradle with rotation axes ϕ and χ used in a neutron pole figure goniometer (Hoefler et al. 1988).

It is also possible to use *position-sensitive detectors* which record intensities along a ring (1 dimension, 1D) rather than at a point. The ring can be mounted on a diffractometer so that it either records for a single reflection a whole range of lattice orientations at once (usually covering the diffractometer coordinates χ, Juul Jensen and Leffers 1989) or

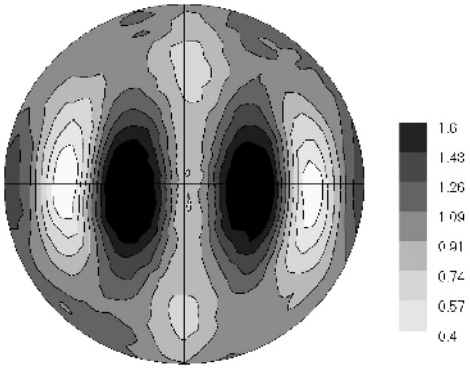

Figure 5. Calcite 0006 pole figure of experimentally deformed limestone, measured with monochromatic neutrons at GKSS, Geesthacht. Equal area projection, linear contours, pole densities in m.r.d. (Compare with Fig. 12).

so that it records a continuous 2θ range (Bunge et al. 1982). The latter is particularly interesting because it permits one to record many pole figures simultaneously and opens the possibility to deconvolute spectra that is valuable in the case of overlapping peaks. The geometry of such a system used at ILL is illustrated in Figure 6. Note that different positions on the detector record differently oriented lattice planes (Bunge et al. 1982). Figure 7 is a graphic representation of 72 spectra measured with a position sensitive detector at different sample orientations for the same experimentally deformed calcite limestone illustrated in Figure 5 (Wenk 1991). The relative changes in peak intensities are due to texture.

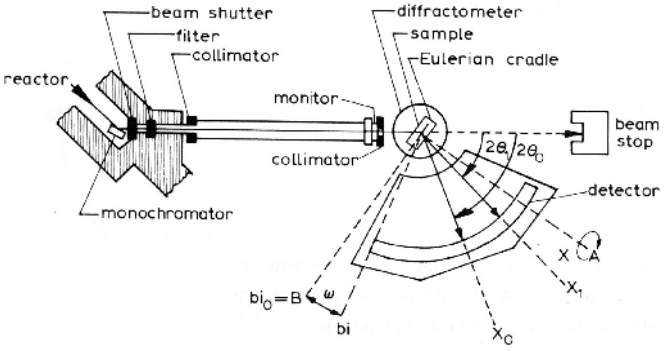

Figure 6. Diffraction geometry for a diffractometer with monochromatic radiation and a position sensitive detector, as for beamline D1B at ILL. The "banana" detector extends over a 2θ range of 80°.

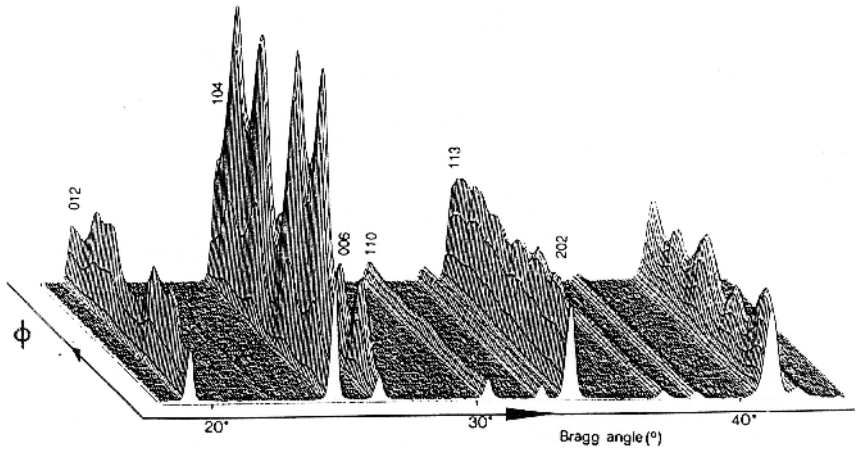

Figure 7. 72 neutron diffraction spectra measured on an experimentally deformed calcite polycrystal (limestone) with a position sensitive detector at ILL with monochromatic neutrons; changes in intensity as a function of ϕ are due to texture (Wenk 1991).

Polychromatic time-of-flight neutrons

Another method to measure a spectrum simultaneously is at a fixed detector position but with *polychromatic* neutrons and a detector system that can identify the energy of neutrons, e.g., by measuring the time of flight (TOF). Figure 8 is a representation of Bragg's law for monochromatic and polychromatic neutrons for aluminum. For monochromatic neutrons with a wavelength λ = 1.5 Å a θ-scan (A) can be performed over the θ-range of interest by moving the detector, or the θ-span can be measured simultaneously with a 1D-position sensitive detector. There are peaks at each intersection of line A with the Bragg curves for lattice planes *hkl*. For polychromatic neutrons a whole range of wavelengths between λ_{min} and λ_{max} is available (line B in Fig. 8). A detector at a fixed scattering angle θ (e.g., 45°) records a whole *d*-spectrum for each sample orientation.

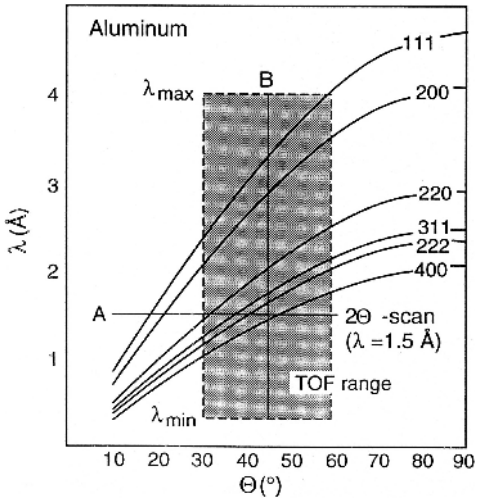

Figure 8. Bragg's law for low order diffractions of aluminum. A illustrates a 2θ scan with a conventional goniometer and monochromatic radiation. B gives the coverage of a continuous spectrum at a fixed detector position. With a position sensitive detector a large 2θ range is measured simultaneously (A) and with an energy sensitive or TOF detector a large wavelength range is covered (B). Both can be combined as with a 2D position sensitive single crystal diffractometer (Fig. 14).

Since neutron scattering is weak, it is efficient to make better use of resources by building instruments with multiple detectors as with SKAT at JINR (24 detectors, Ullemeyer et al. 1998), GPPD at IPNS (14 detectors, Xie et al. 2003) and HIPPO at LANSCE (30 detectors, Wenk et al. 2003). On GPPD detectors are arranged at different angles in the plane of incident and diffracted beam. At SKAT they are positioned in a ring (bank) at right angles to the incident beam (Fig. 9). For HIPPO detectors are arranged on five banks at 2θ angles 10°, 20°, 40°, 90° and 145° (Fig. 19 in Vogel and Priesmeyer 2006, this volume) and each one records reflections from differently oriented lattice planes (*hkl*). The 10° and 20° banks are not used for texture experiments because of poor resolution. The pole figure coverage for 40°, 90° and 145° banks with 30 detectors is illustrated in Figure 10a.

Thus the advantage of pulsed polychromatic neutrons and a detector system that can measure the time of flight (TOF) of neutrons and discriminate their energies is, that whole spectra with many Bragg peaks can be recorded simultaneously. With TOF neutrons and a multi-detector system, fewer sample rotations are necessary to perform quantitative texture analysis. For typical texture investigations with HIPPO, rotation around a single axis is sufficient, which eliminates the need for a 2-circle goniometer and simplifies the construction of environmental cells to measure textures at non-ambient conditions. Rotating the sample around a single axis perpendicular to the incident beam to several positions (0°, 45°, 67.5°, and 90° have been established), provides 4 × 30 = 120 spectra for the subsequent analysis. If detectors are at different θ angles, their resolution is different, which is illustrated in Figure 11 for calcite limestone. High angle detectors (e.g., 145°) have excellent resolution but intensities are weak, particularly at large *d*-spacings. Low angle detectors (e.g., 40°) have poor resolution but good counting statistics. The relative intensity differences between *hkl*'s for different detectors of a bank are indicative of texture (compare with Fig. 7). Combining information from all detectors provides measuring times down to a few minutes per sample. Table 1 compares some features of TOF spectrometers that are used for texture analysis.

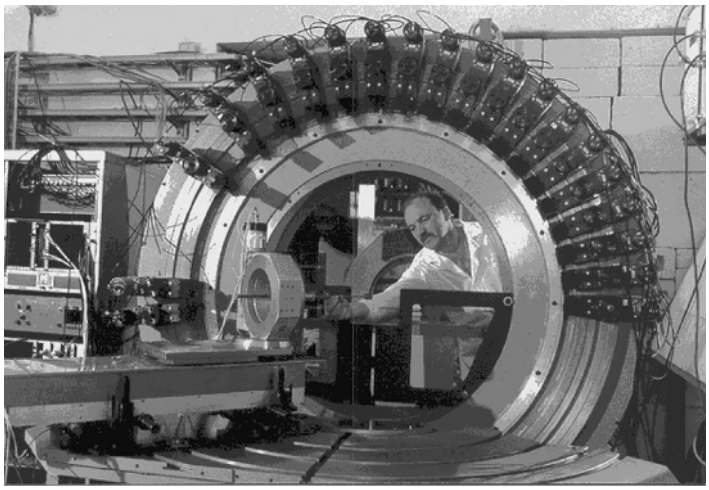

Figure 9. SKAT texture diffractometer at JINR-Dubna with 3 circle goniometer and large ring with detector panels. Person mounting a sample is for scale (courtesy K. Ullemeyer).

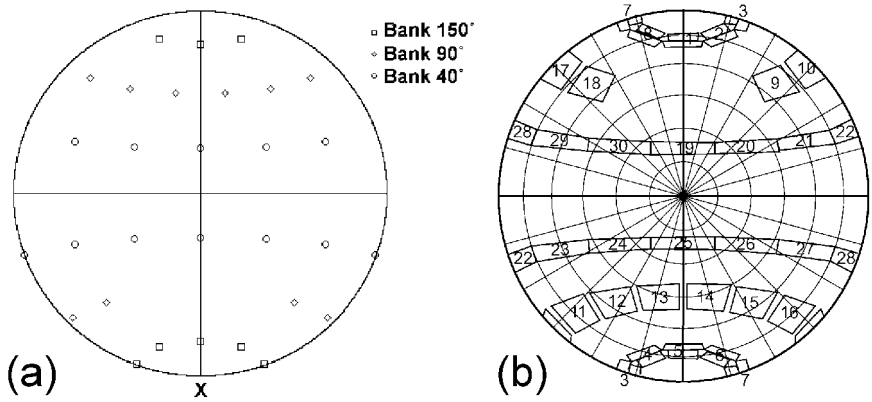

Figure 10. HIPPO pole figure coverage with 30 detector panels, distributed over 3 banks. (a) Point locations of detector centers. X is incident neutron beam. (b) Actual size and shape of detectors. Circles are at 15° intervals. Equal area projection.

The reliability of various neutron texture measurement techniques has been evaluated by circulating a textured polycrystalline calcite standard sample among 15 different neutron diffraction facilities (Wenk 1991; Lutterotti et al. 1997; Von Dreele 1997; Walther et al. 1995; Wenk et al. 2003). They include reactors with monochromatic radiation and point detectors, reactors with position sensitive detectors, pulsed reactors and spallation sources with TOF neutrons. In general textures measured on the same sample at different facilities agree very closely (some examples are shown in Fig. 12). For pole figures with strong diffraction intensities, standard deviations from the mean are 0.04-0.06 m.r.d. with a spread of maxima values of 0.2 m.r.d. The spread is considerably larger for pole figures with weak diffraction intensities (0.4 m.r.d.). For weak diffraction peaks position sensitive detectors and TOF techniques have an advantage over single tube detectors with monochromatic neutrons since integrated rather than peak intensities can be determined which yields better counting statistics.

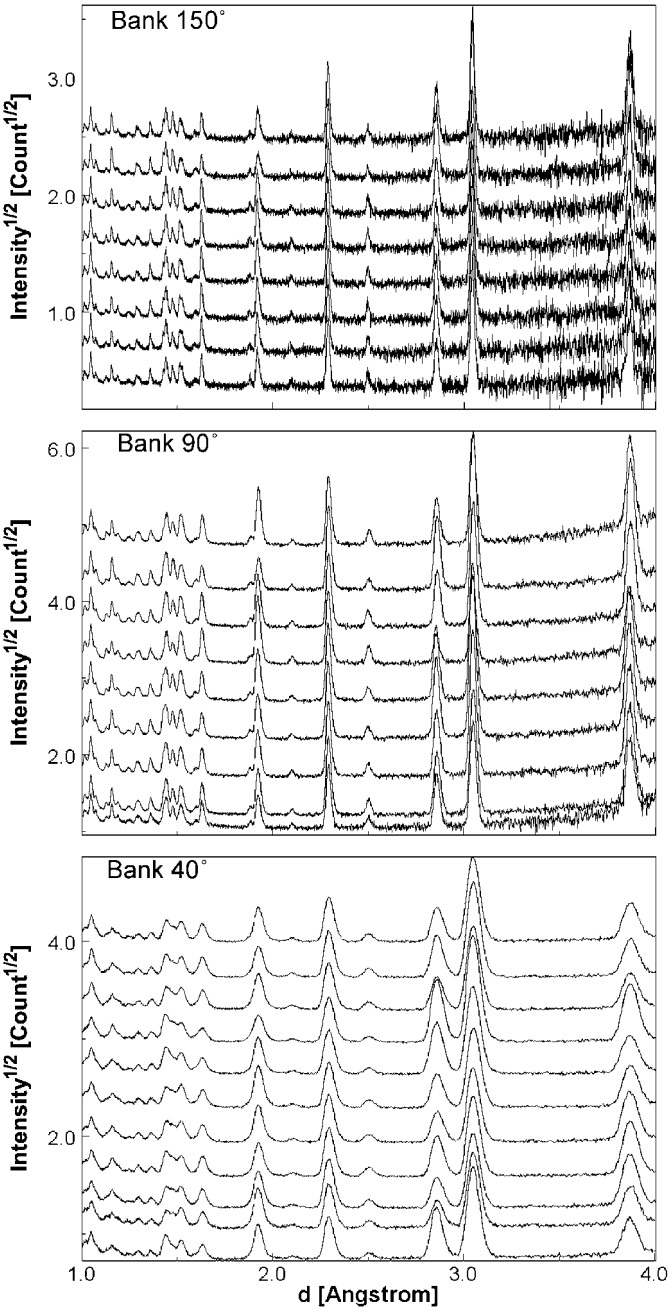

Figure 11. 30 diffraction spectra of calcite limestone, recorded simultaneously with the HIPPO diffractometer at LANSCE. Notice differences in counting statistics and resolution for the different detector banks. Relative peak intensity differences are due to texture (Wenk et al. 2002).

Table 1. Summary of features of neutron TOF spectrometers that are used for texture analysis.

Instrument	Flight path (m)	Flux at sample (neutrons s^{-1} cm^{-2})	Number of detector panels
SKAT (JINR)	103	10^6	24
GPPD (IPNS)	20	3×10^6	14
HIPPO (LANSCE)	9	2.4×10^7	30

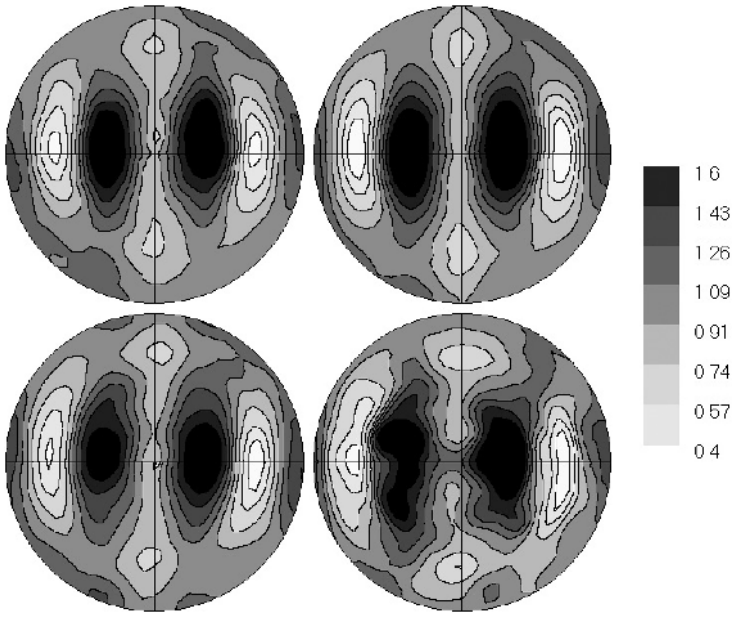

Figure 12. Selected calcite 0001 pole figures of an experimentally deformed limestone standard sample and used as a round robin to assess reliability of neutron diffraction texture measurements. Examples shown are pole figures recalculated from the OD based on measurements at four neutron diffraction facilities. (a) Conventional reactor with monochromatic neutrons (Julios at KFA, Jülich), (b) Reactor with monochromatic neutrons and position sensitive detector (D1B at ILL Grenoble) (Wenk 1991), (c) Pulsed reactor with TOF measurements, single peak extraction (SKAT at Dubna, Russia) (Walther et al. 1995), (d) Spallation neutrons with 30 detectors and OD determined with the Rietveld method (HIPPO at LANSCE) (Wenk et al. 2002). Pole figures are normalized so that densities are expressed in multiples of a uniform distribution (m.r.d.). Equal area projection, linear contours. Compare also with Figure 5.

Results from this round-robin experiment establish that neutron diffraction would clearly be the method of choice for texture measurements of bulk samples if it were more readily available. Quantitative texture information for the same sample obtained by different laboratories with neutron diffraction is much more reproducible than similar comparisons with conventional X-ray diffraction or electron microscopy. This is mainly because of the larger number of grains probed with neutrons, negligible surface preparation effects, and the absence of instrument dependent defocusing and absorption corrections.

Special techniques

This section will briefly discuss some neutron scattering techniques that were explored for special texture applications but have not yet become routine procedures.

2D position sensitive detectors for monochromatic radiation are available at some facilities (e.g., instrument D19 at ILL) and are mainly used for single crystal studies because they cover a significant portion of reciprocal space. This is quite attractive for texture analysis since the 2D diffraction pattern reveals portions of Debye rings for several Bragg peaks and intensity variations along rings can be analyzed for texture. An image is shown for illite clay in Figure 13a. Disadvantages are that the 2D recording is highly distorted in terms of diffraction angle and orientation space, rendering quantitative data extraction difficult. In this respect hard X-ray synchrotron diffraction images are far superior and obtained in a fraction of the time (Fig. 13b, Wenk et al. 2006a).

A similar technique has been investigated earlier by combining 2D position sensitive detectors and TOF (Wenk et al. 1991). With 2D position sensitive detectors as available at the single crystal diffractometers (SCD) of IPNS and LANSCE (Fig. 14), each detector location records a TOF spectrum and the 3D *xyT* data array can then be analyzed for texture. A time slice (T = 6.93 ms) displays Bragg lines of four diffraction peaks with intensity variations (Fig. 15a). Extracting *xy* intensities for d = 2.845 Å, corresponding to (0006) of calcite, provides an angular sector of 25° × 50° for a (0006) pole figure (Fig. 15b). While this technique is quite elegant in principle and has been tested on a few samples (aluminum and calcite), the data analysis is extremely complex due to distortions and non-linear corrections.

With strain neutron diffractometers, samples can be deformed and lattice strains can be recorded *in situ* at stress. Such facilities (e.g., ENGIN-X at ISIS, SMARTS at LANSCE, EPSILON at Dubna) generally have two detectors, recording signals from lattice planes that are

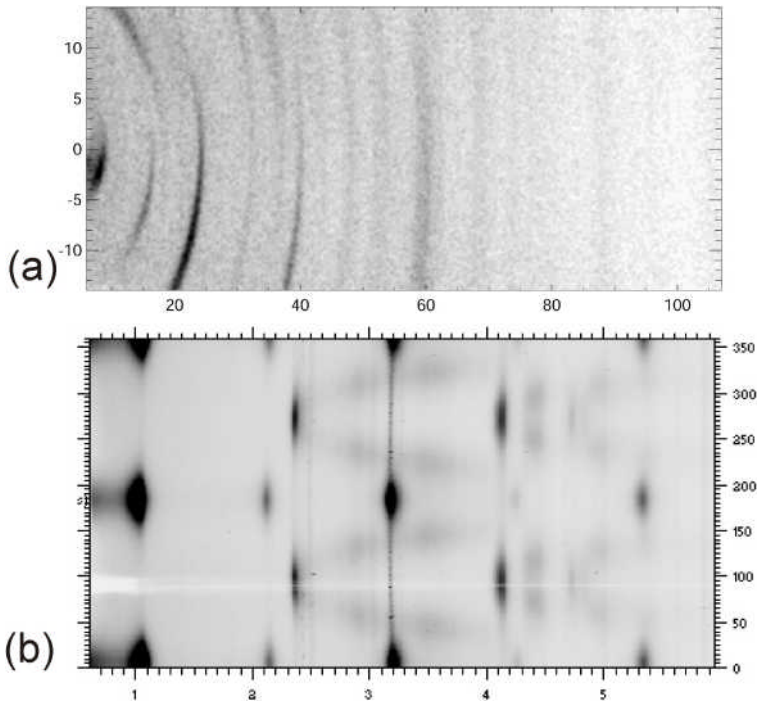

Figure 13. Texture measurements of the clay mineral illite, displaying intensity variations along Debye rings. (a) Position-sensitive neutron detector at D19, ILL; (b) "unrolled" synchrotron diffraction image, recorded with an image plate at HASY (Wenk et al. 2006a). Abscissa corresponds to 2θ angle.

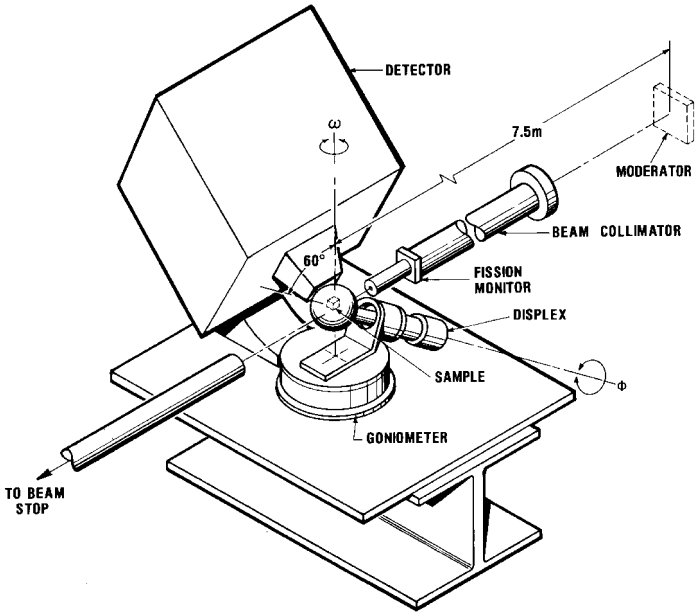

Figure 14. TOF 2D position sensitive detector for single crystal diffractometer (SCD) at LANSCE and IPNS.

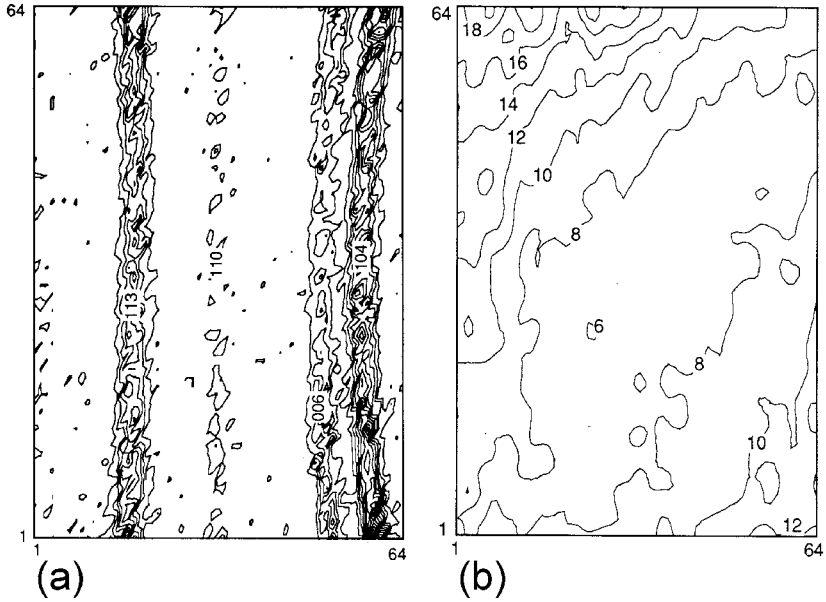

Figure 15. Texture analysis of calcite with the TOF-SCD at LANSCE, displaying the 64 × 64 *xy* division 2D detector. (a) Time slice of the *xyT* histogram with Bragg peaks appearing as high density lines. (b) Extraction of *xy* intensities for d = 2.845 A, corresponding to a segment of the calcite 006 pole figure (Wenk et al. 1991).

oriented perpendicular and parallel to the applied stress. This is generally not sufficient to obtain full texture information, but nevertheless some interesting results have been obtained for calcite (Schofield et al. 2003) and quartz that both undergo mechanical twinning. Polycrystalline quartz, compressed to 500 MPa at 500 °C shows systematic intensity changes of reflections that are sensitive to Dauphiné twinning (e.g., 10-12 and 20-11) and no changes with those that are not (e.g., 11-20) (Fig. 16). These intensity changes are due to texture and reveal that mechanical twinning in quartz initiates around 80 MPa at the conditions of the experiment and saturates around 500 MPa. If the texture of the starting material is known then texture changes during straining can be interpreted quantitatively based on structure factors and intensity changes of reflections.

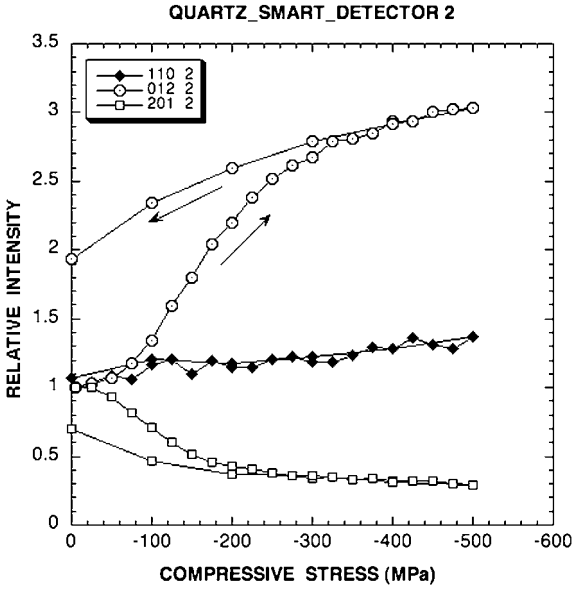

Figure 16. *In situ* observed intensity changes due to mechanical twinning, for several reflections as a sample of quartzite (novaculite) is compressed in the TOF SMARTS strain diffractometer at LANSCE. The detector records lattice planes that are perpendicular to the compression direction.

The neutron cross section of textured materials for certain energies is strongly direction dependent and intensities as function of energy can be used to estimate texture (Santisteban et al. 2006).

DATA ANALYSIS

The goal of texture measurements is to obtain a quantitative 3D orientation distribution (OD), often referred to as ODF (orientation distribution function) since it can be represented as a continuous mathematical function. The OD relates orientations of crystallites (with axes [100], [010] and [001]) to those of the sample (*x, y, z*) usually by means of three Euler angles ϕ_1, Φ, ϕ_2 (Fig. 17a). The 3D OD can not be directly measured with averaging diffraction techniques but methods are available to obtain the OD from measured pole figures (for a review see Kallend 2000). The OD, in terms of Euler angles ϕ_1, Φ, ϕ_2, can be viewed as a cylindrical distribution, with azimuth ϕ_1 and radial distance Φ corresponding to pole figure coordinates, and the axial distance ϕ_2 corresponding to crystal rotation (Wenk and Kocks 1987) (Fig. 17b, top). Pole figures are projections of the OD along complicated paths determined by crystal and sample geometry. A 001 pole figure is simply a projection along the cylinder axis. If several pole figures are measured, the 3D OD can be reconstructed, e.g., using tomographic methods and corresponding software packages are available (POPLA, Kallend et al. 1991; Beartex, Wenk et al. 1998 and others).

For converting relative diffraction intensities to experimental pole figures, it is necessary to apply scaling corrections for incident beam intensity and a subtraction of background intensity. If diffraction peaks are overlapped, they can be integrated and treated as overlapped pole figures

(assigning appropriate structure factor weights), or they can be deconvoluted, fitting them with Gauss functions (e.g., Antoniadis et al. 1990; Merz et al. 1990; Larson and Von Dreele 2004). For both it is advantageous to have position sensitive detectors or use TOF to record continuous spectra. The experimental pole figures can be complete or incomplete and do not need to be normalized. Usually three or four incomplete pole figures are sufficient to determine the OD.

In the traditional approach ODs are determined from pole figure measurements of a *few* diffraction peaks *hkl* in *many* sample orientations. However, rather than to obtain the OD from discrete pole figures, one may want to use directly the diffraction spectra instead. In this case *many* diffraction peaks are used (a continuous spectrum) and thus only a *small* pole figure coverage is required. This corresponds in some ways to calculating the OD from "inverse pole figures" (Morris 1959), though exchange of crystal coverage for sample coverage is limited. The intensity of each diffraction peak in the spectrum also corresponds to a projection of orientation densities along a defined path (Fig. 17b, bottom).

Crystallographers have developed a technique to extract structural information from continuous diffraction spectra (Rietveld 1969; Young 1993; Larson and Von Dreele 2004) and this is the obvious method for TOF data where continuous spectra are measured anyway. An iterative combination of the crystallographic Rietveld profile analysis and OD calculation, proposed by Wenk et al (1994), was implemented for TOF data by Lutterotti et al. (1997) in the software MAUD (Materials Analysis Using Diffraction). It has since been refined (Matthies et al. 2005) and applied to many samples. The Rietveld texture analysis is particularly attractive for low symmetry compounds such as triclinic plagioclase (Xie et al. 2003) and polyphase materials (Wenk et al. 2001; Pehl and Wenk 2005) with many overlapping diffraction peaks. It enables efficient data collection and maximal use of measurements, and provides simultaneously structural and textural information about polycrystals, as well as a quantitative texture correction for crystal structure refinements of textured materials.

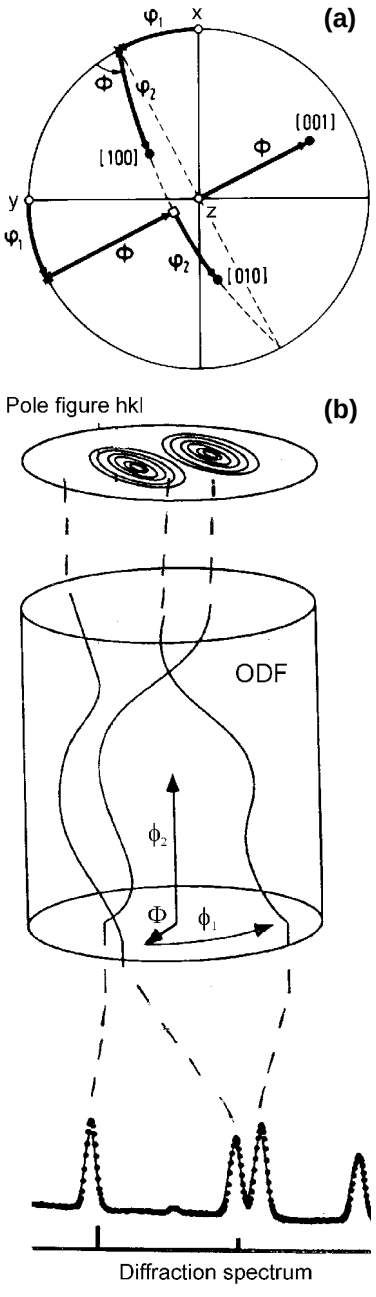

Figure 17. (*to the right*) (a) Euler angles ϕ_1, Φ, ϕ_2 define the orientation of a crystal with axes [100], [010] and [001] relative to a specimen coordinate system *x, y, z*. (b) A three-dimensional orientation distribution (OD), can be represented in a cylinder as function of Euler angles ϕ_1, Φ, ϕ_2. Pole figures are a projection of the OD (top). Also peak intensities of a diffraction spectrum are proportional to projections over OD paths (bottom).

It is pertinent to describe the Rietveld procedure for TOF neutron spectra in some detail and we use the LANSCE HIPPO diffractometer as an example. In the procedure all measured spectra from 30 detector banks and four rotations are taken as input, though only the information within a certain computation range (e.g., 0.8-3 Å) is generally used, yielding many data points (>200,000). Data from a detector bank are usually assumed to represent one point in orientation space (pole figure coverage in Fig. 10a). This is not strictly true because of the finite size of detectors. In HIPPO, for example, each detector has a size of 10-15° (depending on bank) and the actual pole figure coverage is illustrated in Figure 10b with polygons. Because of the detector geometry, the sharpest texture peaks that can be quantitatively represented are 10-15° in width, resulting in an optimal "texture resolution" of 25-30°. (Texture resolution is defined as the capability of quantitatively resolving two adjacent texture components). In principle the resolution could be increased by separating individual detector tubes but this would require much longer counting times and increase the computational effort enormously. For most deformation textures a 25-30° resolution is adequate.

With these diffraction data first instrumental, background, and phase parameters are refined. It is advantageous to calibrate instrumental parameters with a powder standard (such as Si) and obtain accurate values for instrumental peak aberrations that are convoluted with peak broadening due to the sample (e.g., crystallite size, microstrain and microstructure). From the spectra measured on the unknown sample for each detector a scale factor has to be refined to take account of detector efficiency and variations in absorption as neutrons pass through various components of the instrument. These scale factors may vary by a factor of 2 or more. Each detector is at a slightly different flight path, requiring a refinement of deviations from the average. Furthermore sample displacement parameters need to be refined to take account of the fact that the sample center as well as the goniometer rotation axis are usually not exactly aligned in the neutron beam. Next background parameters for each spectrum are determined. The background function is assumed to be a polynomial corrected with the incident spectrum (2^{nd} to 4^{th} order).

Once the background and instrument parameters are refined, crystallographic parameters such as lattice parameters, atomic coordinates and thermal parameters are determined. Now the texture refinement can start and for this several algorithms exist, most notably direct methods that solve the problem with tomography as alluded to above (Fig. 17b), and Fourier methods, generally referred to as "harmonic method" (Bunge 1965, 1982), where pole figures and OD are expressed as harmonic functions (hence ODF, see discussion above). The various methods, implemented in the Rietveld procedure, have recently been compared for TOF measurements of extruded aluminum with a strong and asymmetric texture (Matthies et al. 2005) and in Figure 18 001 pole figures recalculated from the OD are shown. The texture peak (above 1 m.r.d.) is similar in all pole figures but there are considerable differences for the region below 1 m.r.d. that constitutes nevertheless a large part of orientations. The tomographic method WIMV (Matthies and Vinel 1982), modified to permit irregular data coverage, provides smooth pole figures that are positive throughout (Fig. 18a). The harmonic method displays similar peaks, but considerable oscillations in the lower pole density regions, including slight negative deflections, for a harmonic expansion to $L_{max} = 12$ (Fig 18b). The pattern becomes considerably worse for $L_{max} = 16$ with many negative oscillations and exaggerated maxima (9.5 m.r.d.) (Fig. 18c).

We find that harmonic methods are adequate for a qualitative description of the main texture component. Due to the limited resolution of detectors and incomplete pole figure coverage, harmonic expansions beyond $L_{max} = 12$ introduce subsidiary oscillations, which are artifacts. The results from this analysis of aluminum illustrate the well-known limitations of the harmonic method: termination errors and lack of odd coefficients. Of the two currently available Rietveld programs that incorporate texture analysis, only MAUD (Lutterotti et al. 1997) includes discrete methods. GSAS (Von Dreele 1997) is limited to harmonic algorithms. Both do not incorporate any of the sophisticated approaches to extract odd coefficients in the harmonic expansion (e.g., Dahms and Bunge 1988; Van Houtte 1991). Even though

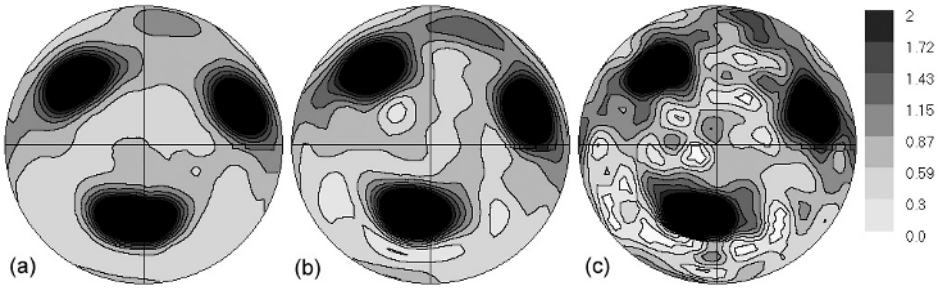

Figure 18. 100 pole figures recalculated from the OD of extruded aluminum, measured with the TOF diffractometer HIPPO and analyzing spectra with the Rietveld method. (a) Obtained with the tomographic method EWIMV, (b) Harmonic method with series expansion to $L_{max} = 12$, (c) series expansion to $L_{max} = 16$. Equal area projection, linear contour scale, pole densities in m.r.d. White regions are below zero (Matthies et al. 2005).

computationally straightforward, it turns out that limited detector resolution and irregular data coverage are much more serious for harmonic than discrete methods.

How much confidence can we have in a Rietveld refinement? A first indication is the value of a bulk R-factor that compares measured and refined values. However, particularly for 3D textures, such a single number is not adequate to reveal all possible shortcomings of the model. It is necessary to compare individual spectra and assess deviations. Figure 19 shows measured data (dots) and calculated spectrum (line) for calcite. A fit as illustrated here for a 90° detector is adequate. However, this is just one out of 40 90° detector spectra. An overall assessment is best provided by a "mapplot" that stacks all spectra and represents intensities with gray shades (Fig. 20). The lower part are measured spectra, the top part recalculated ones. Also here the similarity, both of peak intensities and their variation, as well as background intensities are very similar, giving us confidence that the refinement is good.

With multidetector systems such as HIPPO and data analysis with the Rietveld method neutron texture analysis has become a routine. An automatic sample changer can measure up

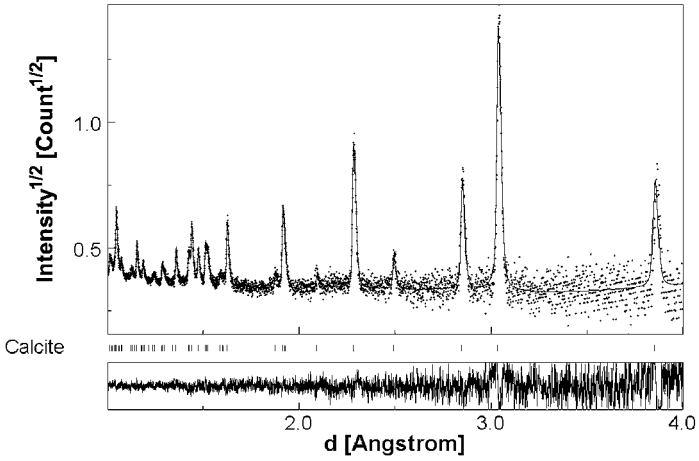

Figure 19. A typical spectrum of calcite measured with the TOF HIPPO diffractometer (150° bank detector panel). Dots are measured data and line is the fit obtained with the Rietveld code MAUD. Deviations (bottom) are minimal and largely due to counting statistics which is worst for large *d*-spacings.

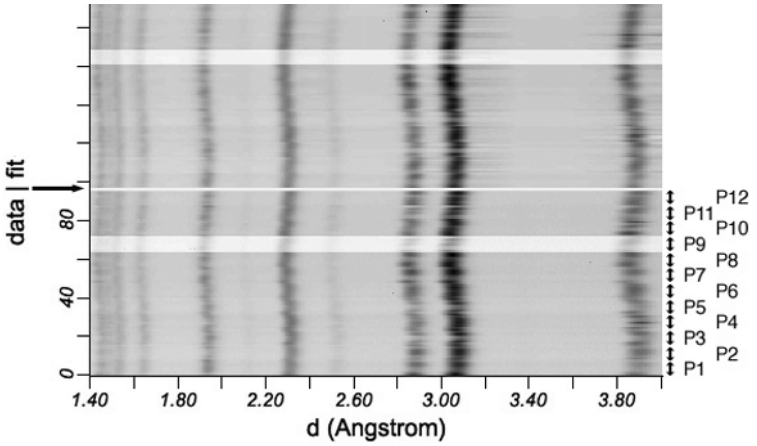

Figure 20. Limestone round robin standard measured with HIPPO and analyzed with the Rietveld method. Mapplot illustrating with gray shades intensity variations for 12 detectors of the 90° bank and 8 sample rotations. Bottom are measured data and top is the Rietveld fit. Note the excellent reproduction of background and peak intensities as well as peak positions. The wavy *d*-spacing variation is due uncertainties about the sample position relative to detectors (Wenk et al. 2002).

to 32 samples without intervention of the instrument scientist. Textures can be measured *in situ* at temperature, stress (CRATES) and pressure, opening the field to investigate texture changes in representative sample volumes, e.g., during phase transformations or recrystallization. But TOF multidetector systems have also their drawbacks. The average flightpaths from sample to detector has to be calibrated with an external standard of different geometry than the actual sample and thus needs to be refined, introducing uncertainty. Also the representative sample center may be displaced during rotations. Processing of the data recorded by the 30 detector panels on 720 detector tubes with 4,136,113 TOF channels is not only complex but intensities also are subject to electronic instabilities and may vary slightly over the duration of an experiment. And counting statistics for high angle detectors and large *d*-spacings that contain diagnostic reflections in many minerals is poor, with much uncertainty about spectral corrections. None of these limitations is critical and can generally be refined, but the investigator has to be aware of all the possible complications that may affect data quality.

APPLICATIONS

Compared with X-ray pole figure diffractometry and electron backscatter diffraction patters (EBSP), the number of texture analyses by neutron diffraction is small. The main reason for this is the limited access to neutron facilities and long delays in obtaining beamtime. For those who need texture results right now, neutron diffraction is not the best method. Another reason is the involved data processing procedure that requires expertise. To obtain an OD from pole figures or EBSP data is a matter of minutes, for neutron diffraction, particularly when using the Rietveld technique, it still takes hours or even weeks in the case of complex materials. Thus it is no surprise that for materials with strong and well separated diffraction peaks (cubic and hexagonal metals, quartz, calcite) conventional methods are adequate and there is no need to write proposals, wait for approval, travel to distant facilities, just to measure a few samples. Similarly the cost of neutrons does not justify experiments on such materials. Yet there are cases where neutrons have distinct advantages and, interestingly, many of these applications are in earth sciences. Neutrons are essential for low symmetry crystals (such as

triclinic plagioclase: Wenk et al. 1985; Ullemeyer et al. 1994; Xie et al. 2003) and polyphase materials, including many rocks (Dornbusch et al. 1994; Siegesmund et al. 1994; Helming et al. 1996; Gastreich et al. 2000; Wenk et al. 2001; Leiss et al. 2002; Kurz et al. 2004; Ivankina et al. 2005; Pleuger et al. 2005) with closely spaced and partially overlapping diffraction peaks. For such materials conventional pole figure goniometry cannot be used.

Grain statistics

As was pointed out earlier, grain statistics can be important (Figs. 2 and 3) and neutron diffraction that analyzes large sample volumes has distinct advantages in characterizing bulk materials. This is particularly relevant for ore minerals that have been investigated extensively. Pyrite (Jansen et al. 1992; Siemes et al. 1993), chalcopyrite (Jansen et al. 1993, 1996a,b), pyrrhotite (Niederschlag and Siemes 1996), galena (Skrotzki et al. 2000) and hematite (Rosière et al. 2001; Guenther et al. 2002; Siemes et al. 2003; Hansen et al. 2004) are often coarse-grained and only analyzing large volumes provides adequate statistics. This is significant for estimating the anisotropy of physical properties such as magnetic susceptibility (Siemes et al. 2000; Fig. 21). Similar considerations apply to iron meteorites, where orientation relations between phases in Wiedmanstätten patterns, and volume fractions of orientation variants for bcc lamellae of kamacite are elegantly determined with neutron diffraction (Höfler et al. 1988; Fig. 22).

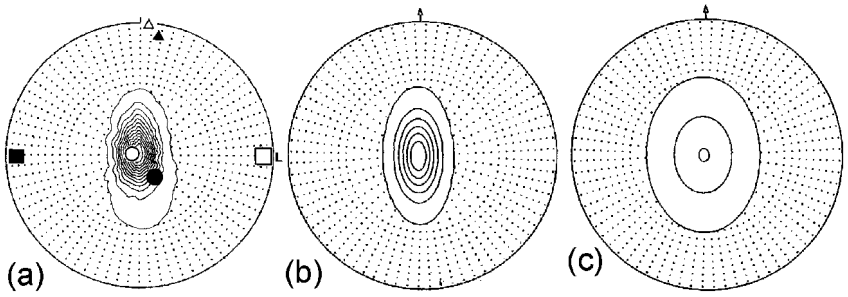

Figure 21. Measured and modeled 0003 pole figures of hematite from the Andrade mine, Brazil. (a) Experimental pole figure measured by neutron diffraction . Closed symbols are measured principal axes of magnetic susceptibility, open symbols are calculated axes. (b) Modeled pole figure based on a Bingham distribution to fit experimental pole densities and (c) modeled pole figure to fit measured susceptibilities (Siemes et al. 2000).

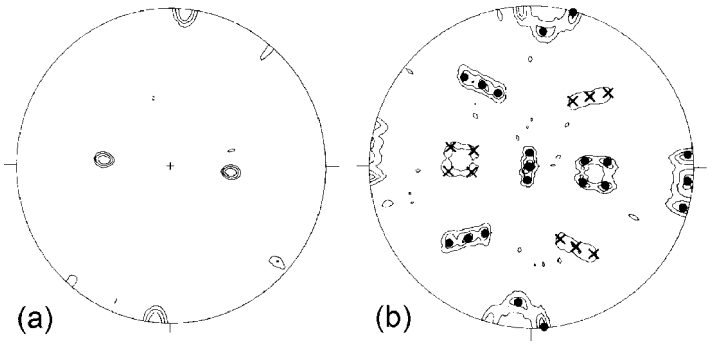

Figure 22. Pole figures of the Gibeon octahedrite meteorite measured by neutron diffraction at Jülich. This sample shows Widmanstätten patterns with intergrowth of fcc taenite and bcc kamacite. (a) (200) pole figure of taenite, (b) 200 pole figure of kamacite. Symbols indicate ideal orientations for a Nishiyama-Wassermann relationship between bcc and fcc phases. The variants with dots are emphasized over the variants with crosses (Höfler et al. 1988).

Statistical considerations also apply if textures are weak and large volumes are needed to establish significant patterns, as in the case of quartz that was deformed by a shock wave from a meteorite impact (Wenk et al. 2005), in fine-grained carbonates in deep sea sediments (Ratschbacher et al. 1994) and halite (Skrotzki et al. 1995). The good statistics was crucial in establishing anisotropy in calcite marble used as building materials (De Wall et al. 2000; Leiss and Weiss 2000; Siegesmund et al. 2000; Zeisig et al. 2002). This latter case is interesting since it represents a new application for texture analysis of rocks. Because of the anisotropy of thermal expansion of calcite, certain directions in textured marbles are most susceptible to microfracturing and spallation during seasonal temperature changes and the sectioning of slabs ought to take preferred orientation into account (Fig. 23).

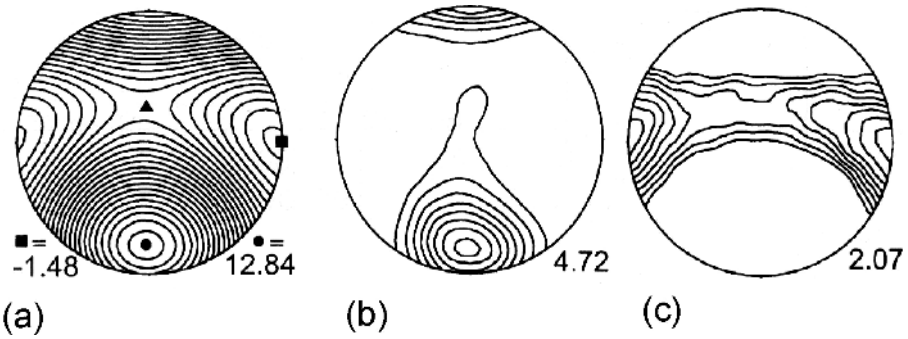

Figure 23. Fabric anisotropy in Carrara marble. (a) Dilatation coefficient a (in 10^{-6} C^{-1}) calculated from the texture; (b) 0006 and (c) $11\bar{2}0$ pole figures measured by neutron diffraction on spherical samples of 30 mm diameter at Dubna, maxima (in m.r.d.) are indicated. Equal area projection (Leiss and Weiss 2000).

Polymineralic rocks

Increasingly textures determined by neutron diffraction are being used in the interpretation of geologic deformation histories (Leiss et al. 1999; Ullemeyer and Weber 1999; Leiss and Molli 2003; Pleuger et al. 2005), as well as the interpretation of seismic anisotropy in the crust (Ivankina et al. 2005; Ullemeyer et al. 2006). Preferred orientation of quartz has been of prime interest in petrofabric research, ever since the first pole figure was published by Schmidt (1925). Quartz textures have been measured in many rocks and the great variety of fabric types was classified by Sander (1950). Until recently most of this research relied on Universal stage measurements, which can only determine orientations of the c-axes. Also today most discussions of quartz textures emphasize (0001) pole figures. Neutron diffraction has been used to establish the full crystal orientation distribution that provides important additional geological information about the deformation history.

The case is granitic mylonites, rather common highly deformed quartz-bearing rocks. Neutron diffraction is preferred because these rocks contain several phases (mainly quartz, plagioclase feldspar and biotite mica), and because they are fairly coarse-grained. Only a volume average can provide adequate statistics. Pehl and Wenk (2005) investigated textures of mylonites from the Santa Rosa mylonite zone in southern California by TOF neutron diffraction, analyzing data with the Rietveld method. Figure 24 shows a spectrum with the Rietveld fit, documenting a large number of diffraction peaks, many of them overlapped. With the Rietveld method volume fractions could be refined (quartz: 38 vol%, plagioclase: 50 vol%, biotite 12 vol%), as well as orientation distributions for the three phases. The plagioclase texture is more or less random, biotite has a very strong texture. Only quartz will be discussed here. Figure 25a displays pole figures recalculated from the OD. They are projected on the foliation plane, with

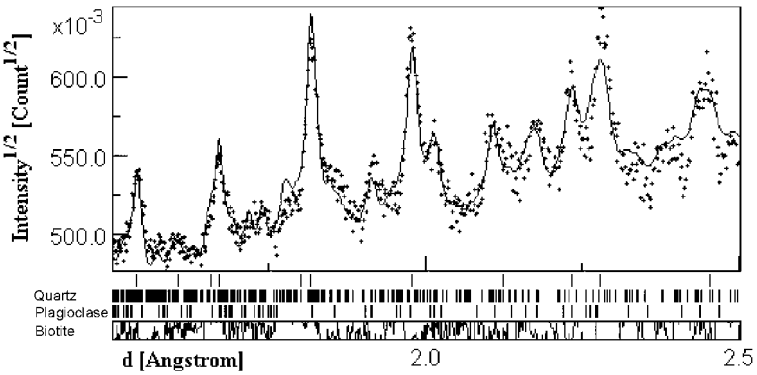

Figure 24. Rietveld fit (line) of a HIPPO TOF spectrum (dots) of granitic mylonite with three principal phases quartz, plagioclase and biotite (90° detector).

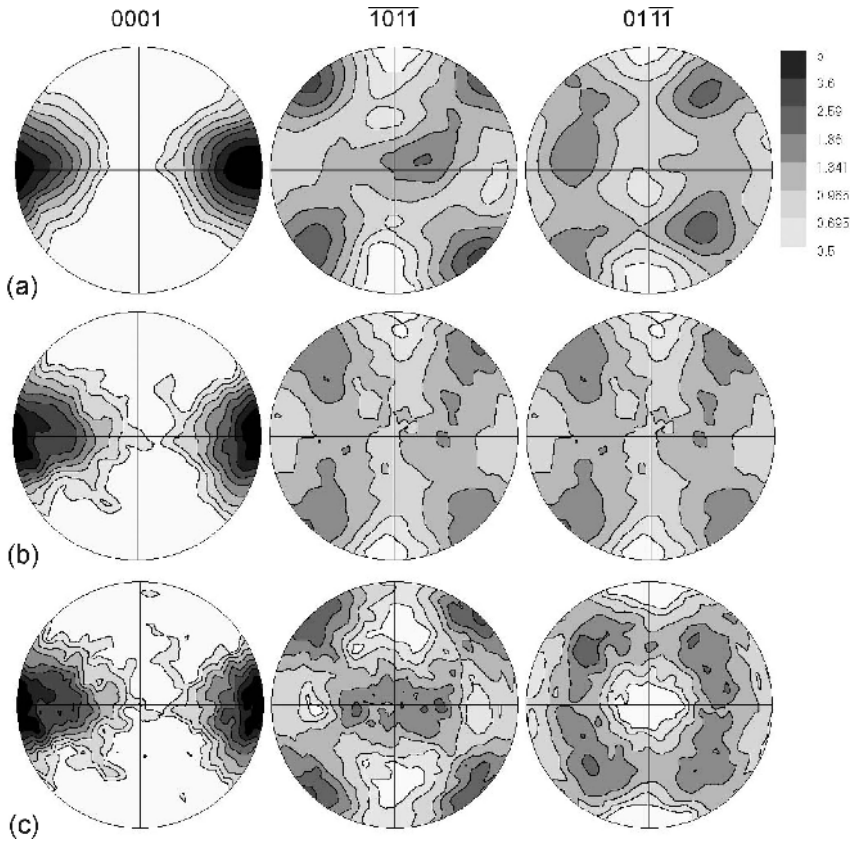

Figure 25. Quartz in mylonite of granitic composition from Palm Canyon, California. (a) Pole figures recalculated from the OD using neutron diffraction and Rietveld method. (b) Discretization of OD and applying Dauphiné twinning to all orientations. (c) Imposing compression in the center (pole of foliation) and inducing Dauphiné twinning to minimize elastic energy. Equal area projection, logarithmic contours, pole densities in m.r.d. (Pehl and Wenk 2005).

the lineation direction vertical. By analyzing many samples, the authors showed that this texture is fairly constant over 20 km and thus representative of tectonic deformation. The *c*-axis pattern with a maximum in the foliation plane at right angles to the lineation is typical of dynamic recrystallization; *a*-axes align preferentially in the lineation direction.

Of particular interest are the patterns for positive rhombs $\{10\bar{1}1\}$ and negative rhombs $\{01\bar{1}1\}$. They are different and furthermore have a lower symmetry than the orthorhombic $c = (0001)$ and $a = \{11\bar{2}0\}$ pole figures. The two rhombs are related by Dauphiné twinning, with host and twin related by a 2-fold rotation about the *c*-axis. Indeed mechanical twinning under stress and due to the large elastic anisotropy of quartz may have introduced this pattern. The effects of twinning can be modeled by first applying it to all orientations (Fig. 25b). This does not affect *c*- and *a*-axes, and positive and negative rhombs become equal. Now a compressive stress is applied perpendicular to the foliation (center of pole figure) and Dauphiné twinning is induced to minimize the elastic energy. It produces the texture pattern in Figure 25c. This pattern has a great similarity with the observed texture (Fig. 25a), suggesting that mechanical twinning did indeed occur and can thus be used as a paleopiezometer. Mechanical twinning in quartz rocks initiates around 80 MPa (Fig. 16). Deviations of rhombohedral pole figures from orthorhombic symmetry are attributed to a component of non-coaxial deformation.

Interestingly it has been found that with increasing deformation quartz-bearing mylonites become susceptible to the alkali silica reaction if used as aggregate in concrete and render such concrete very unstable (Monteiro et al. 2001). This is probably due to intracrystalline deformation of quartz and with neutron diffraction texture analysis the overall deformation state of the rock can be assessed (Wenk and Pannetier 1990) and its suitability as aggregate material established.

In situ experiments and phase transformations

So far all examples were investigated at ambient conditions. However, neutron diffraction offers the possibility to record texture changes *in situ* at temperature, pressure and stress. The HIPPO diffractometer at LANSCE is unique by the availability of furnaces, cryostats, pressure cells and straining devices that are compatible with texture measurements. The trigonal (α)-hexagonal (β)-trigonal phase transformation of quartz in quartzite is used to illustrate this capability. A cylinder of mylonitic quartzite, 1 cm in diameter, is heated in a vacuum furnace. At 300 °C the texture pattern is roughly trigonal, with a *c*-axes maximum and three concentrations of rhombs (Fig. 26a). Upon heating to 625 °C the texture becomes hexagonal with no changes to *c*-axes or *a*-axes (Fig. 26b). The phase transformation is displacive and reversible, with only minor distortions of bonds. Upon cooling each crystal could choose between two orientation variants, related by a 180° rotation about the c-axis. It turns out that there is a perfect memory and the texture reverts exactly to the initial pattern (Fig. 26c). The cause of this texture memory is not yet understood but qualitatively attributed to the effect of stresses imposed by neighboring grains.

Similar heating experiments have been performed on metals documenting texture changes during recrystallization and a less perfect texture memory in the hcp→bcc→hcp transformation of zirconium (Wenk et al. 2004) and the bcc→fcc→bcc transformation of iron (Wenk et al. 2006b). Such *in situ* texture measurements may help us to better understand anisotropy changes during phase transformations and particularly variant selection in martensitic transitions. In titanium Bhattacharyya et al. (2006) could document that during the phase transformation preexisting bcc grains grow, replacing hcp orientations.

To end our discussion of examples we go to low temperature. With neutron diffraction it is possible to investigate textures of ice that is not only relevant on earth but also for the outer planets where high pressure forms of ice control their rheology. For neutron diffraction it is necessary to use deuterated ice to avoid strong inelastic scattering (see also Kuhs and

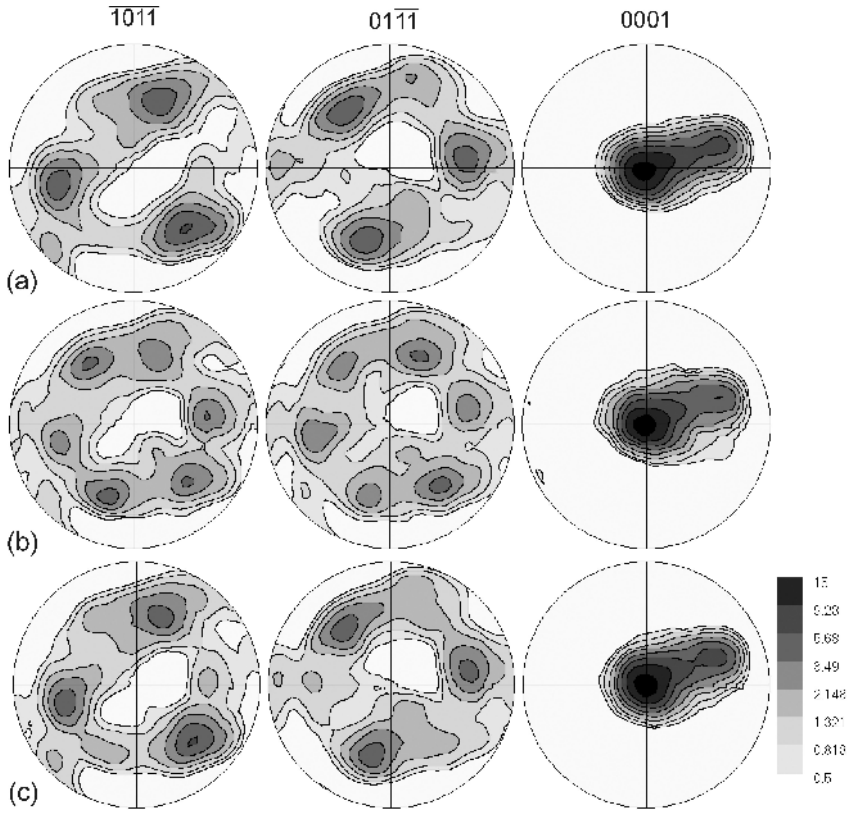

Figure 26. Mylonitic quartzite, measured *in situ* at different temperatures with the TOF diffractometer HIPPO. (a) 300 °C, (b) 625 °C (above the hexagonal phase transformation), (c) 300 °C (after cooling). Note the perfect texture memory. Equal area projection, logarithmic contour scale, pole densities in m.r.d.

Hansen 2006, this volume). The experimental study of Bennett et al. (1994) documented for hexagonal ice I pole figures with *c*-axes parallel to the compression direction (Fig. 27a) and for rhombohedral high pressure ice II *c*-axes perpendicular to the compression direction, indicating different deformation mechanisms (Fig. 27b).

Magnetic textures

Harrison (2006, this volume) discussed the unique magnetic scattering of neutrons. This was the original incentive for Brockhouse (1950) to use neutrons for texture analysis. There have been several attempts to determine magnetic textures, i.e., the orientation of magnetic domains (e.g., Henning et al. 1981; Zink et al. 1994, 1997; Birsan et al. 1996). As was outlined by Bunge (1989) different situations may arise in magnetic materials: In demagnetized ferromagnetic materials such as cubic iron magnetic moments may be oriented randomly in any of the six <100> directions. In this case the crystallographic and magnetic texture are identical. A weak magnetic field produces a preferential alignment of moments along certain <110> directions destroying the cubic crystal symmetry. Birsan et al. (1996) conducted an interesting study on silicon steel. The 110 pole figure of the demagnetized material, measured by neutron diffraction (Fig. 28a), corresponds to a typical rolling texture. A difference pole figure subtracting the demagnetized pole figure from the pole figure with an applied magnetic field in the rolling direction (center) is shown in Figure 28b. The magnetic part of neutron

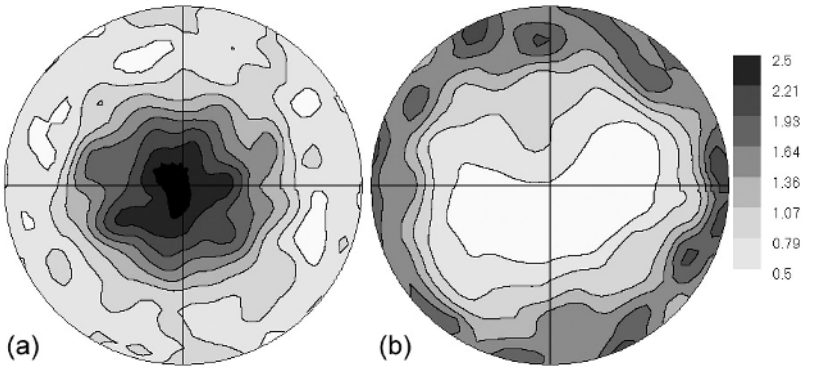

Figure 27. (0001) pole figures of ice deformed experimentally in axial compression (compression direction in center). (a) Hexagonal ice I. (b) Rhombohedral high pressure polymorph ice II. Equal area projection, linear scale, pole densities in m.r.d. (Bennett et al. 1994).

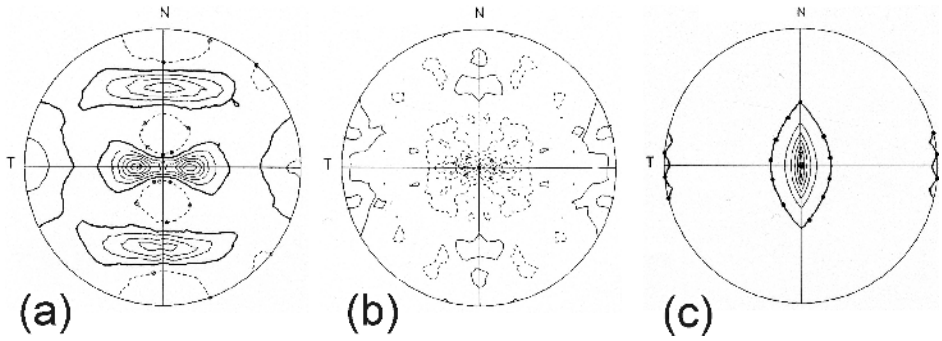

Figure 28. Magnetic silicon steel investigated by neutron diffraction. (a) (110) pole figure of demagnetized steel, (b) difference pole figure (magnetized, 150 mA-demagnetized) illustrating magnetic scattering, (c) magnetic texture of the magnetized sample obtained by modeling (Birsan et al. 1996).

scattering has a minimum in the center and concentrations near the transverse direction. It can be used to determine, through modeling, the magnetic pole figure, i.e., the alignment of magnetic moments (Fig. 28c) which turns out to be more or mess parallel to the {100} maxima of easy magnetization and the magnetic field. In high magnetic fields the magnetization is no longer related to a crystallographic direction and thus becomes independent of the crystallographic texture.

To our knowledge there are no applications to minerals but studies of magnetic textures of ferrimagnetic mineral ores such as manganite and magnetite could reveal informative distributions to assess paleomagnetic properties of rocks.

New possibilities

Classical applications of neutron diffraction texture analysis to coarse materials, improving grain statistics, and to low-symmetry polyphase materials were discussed. Also mentioned were *in situ* experiments at high and low temperature. There is a wealth of other possibilities to use neutron diffraction to characterize direction-dependent properties. Texture patterns may be compared with strain pole figures that display elastic deformation (Wang et al. 2002, 2003), either caused by applied stress or expressing residual stress. Such directional stress measurements are barely explored for geological materials (Darling et al.

2004; Schofield et al. 2003; Daymond 2006, this volume). This opens exciting possibilities for quantitative modeling, combining textures, lattice strain, stored energy (Hayakawa et al. 1997) and microstructure to better understand material-forming processes (Agnew et al. 2003; Brown et al. 2003, 2005). Much of this is promoted by metallurgists but similar theories are also applied to understand deformation of rocks (for a review e.g., Wenk 1998).

COMPARISON OF METHODS AND RECOMMENDATIONS

The optimal choice of pole-figure measurements depends on many variables, such as availability of equipment, material to be analyzed, and data requirements.

Neutron diffraction is advantageous for determination of complete pole figures in coarse-grained aggregates and, in principle, allows determination of magnetic pole figures. The advantage of neutrons is that bulk samples rather than surfaces are measured, that coarse grained materials can be characterized, that environmental cells (heating, cooling, straining) are available and that resolution in d is much better than with conventional X-ray pole figure goniometers in reflection geometry where peak broadening occurs because of defocusing effects with sample tilt. This makes it possible to measure complex composites with many closely spaced diffraction peaks. With position sensitive detectors, and particularly with TOF, continuous spectra can be recorded; shifts in peak positions can be used for residual stress determination and intensities to extract simultaneously texture information, for example with the Rietveld method.

For routine metallurgical practice and many other applications in materials science and geology, *X-ray diffraction* with a pole figure goniometer in back-reflection geometry is generally adequate. It is fast, easily automated, inexpensive both in acquisition and maintenance. X-ray diffraction texture analysis done on a flat surface is restricted to fine-grained materials (<1 mm) that are homogeneous within the plane. Back reflection provides only incomplete pole figures, but this drawback can be overcome by data analysis. Pole figures can only be measured adequately if diffraction peaks are sufficiently separated. In geological samples and ceramics, X-ray diffraction is therefore generally limited to single phase aggregates of orthorhombic or higher crystal symmetry.

Electron diffraction with a *TEM* is most tedious but provides valuable information about dislocation microstructures and, at least two-dimensionally, about interaction between neighbors and about heterogeneities within grains (e.g., Schwarzer and Weiland 1988). This is important data to interpret deformation processes.

Electron Backscatter Diffraction Patterns (EBSP or *EBSD)*, measured with the *SEM* and produced on polished surfaces, can be used to determine local orientation and this technique has become an important addition to the methods of texture measurements (Lloyd et al. 1991; Randle and Engel 2000). While such measurements do not provide direct information on dislocation microstructures, they allow for determination of local orientation correlations that are important in the study of recrystallization or of stress concentrations on which failure may occur. It can be used to produce orientation maps (OIM, Orientation Imaging Microscopy, Adams et al. 1993). Determination of individual grain orientations has advantages for OD calculations because of the absence of ambiguity, which is inherent in pole figures. With the possibility of automation this technique has become comparable in expense and effort to X-ray diffraction analysis. It remains confined to samples of fairly high crystallinity and moderate deformation. Figure 29 compares pole figures of quartz obtained by EBSP (Fig. 29a) and neutron diffraction (Fig. 29b). They are virtually identical (Kunze et al. 1994) but for the neutron data, measured on a 1cm cube, they represent the actual data, for the EBSD results they had to be arbitrarily smoothed with a 15° filter to obtain the same pole densities.

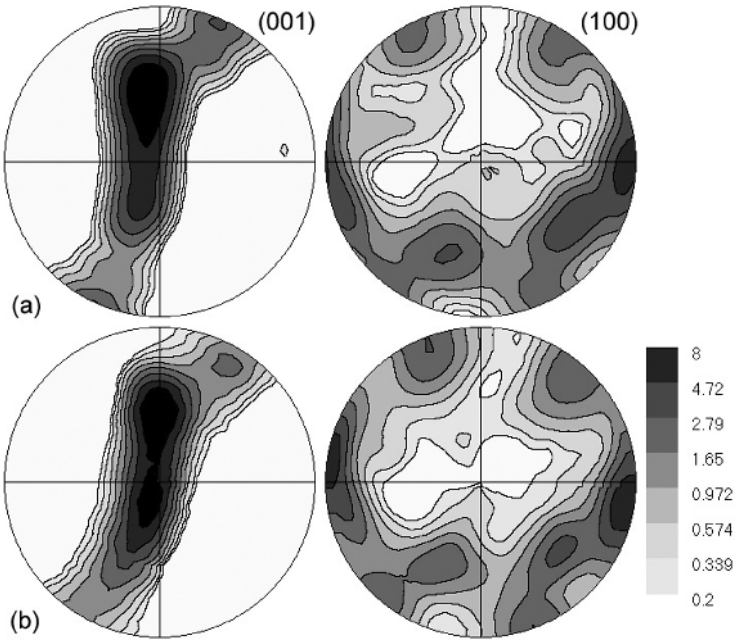

Figure 29. Naturally deformed mylonitic quartzite. Pole figures obtained from (a) EBSP measurements in the SEM and arbitrary smoothing with a 15° Gauss filter and (b) by neutron diffraction with a monochromatic source at Jülich and recalculated from the OD. Equal area projection, linear contours, pole densities in m.r.d. (Kunze et al. 1994).

A new technique is to use *hard X-rays* ($\lambda \sim 0.1$ Å) produced in a *synchrotron* and record 2D diffraction images with image plates or CCD cameras. Such high energy X-rays can penetrate several millimeters of thickness and thus have become comparable to neutrons as far as volume averages are concerned (Wenk and Grigull 2002). Synchrotron X-rays have the advantage of very high intensity. It is likely that they will replace neutrons for some applications, particularly if only grain size and resolution are issues. Similar Rietveld techniques are applied to obtain quantitative texture information from 2D images as from 1D neutron spectra (Lonardelli et al. 2005).

This Chapter has reviewed methods of texture analysis by neutron diffraction, an increasingly important application of neutron scattering. Those interested in preferred orientation and how it relates to macroscopic anisotropy of physical properties as well as deformation history and rheology should consult the literature (e.g., Wenk 1985; Kocks et al. 2000; Karato and Wenk 2002).

ACKNOWLEDGMENTS

Neutron scattering was a wonderful opportunity to meet people from a wide variety of fields, starting with the first experiments in 1980 at Jülich with W. Schäfer and ILL with H.-J. Bunge and J. Pannetier, and more recently the close interaction at Los Alamos around HIPPO with K. Bennett, R. Von Dreele, A. Hurd and S. Vogel. I am grateful to reviewers for their comments, particularly Sven Vogel and Mark Daymond and contributions from H.-G. Brokmeier, W. Schäfer and K. Ullemeyer. Research was supported by several agencies, foremost NSF, DOE and IGPP.

REFERENCES

Adams BL, Wright SI, Kunze K (1993) Orientation imaging: The emergence of a new microscopy. Metall Trans 24A:819-831

Agnew SR, Tomé CN, Brown DW, Holden TM, Vogel SC (2003) Study of slip mechanisms in a magnesium alloy by neutron diffraction and modeling. Scripta Mater 48:1003-1008

Antoniadis A, Berruyer J, Filhol A (1990) Maximum-likelihood methods in powder diffraction refinements. Acta Cryst A46:692-711

Bennett K, Wenk H-R, Durham WB, Stern L, Kirby SH (1997) Preferred crystallographic orientation in the ice I→II transformation and the flow of ice II. Philos Mag A 76:413-435

Bhattacharyya D, Viswavathan GB, Vogel SC, Williams DJ, Venkatesh V, Fraser HL (2006) A study of the mechanism of α to β phase transformation by tracking texture evolution with temperature in Ti-6Al-4V using neutron diffraction. Scripta Mater 54:231-236

Birsan M, Szpunar JA, Tun Z, Root JH (1996) Magnetic texture determination using nonpolarized neutron diffraction. Phys Rev B 53:6412-6417

Brockhouse BN (1953) The initial magnetization of nickel under tension. Can J Phys 31:339-355

Brokmeier H-G (1997) Neutron diffraction texture analysis. Physica B 234-236:977-979

Brokmeier H-G (1999) Advantages and applications of neutron texture analysis. Textures Microstructures 33: 13-34

Brown DW, Abeln SP, Blumenthal WR, Bourke MAM, Mataya MC, Tomé CN (2005) Development of crystallographic texture during high rate deformation of rolled and hot-pressed beryllium. Metall Mater Trans 36A:929-939

Brown DW, Bourke MAM, Clausen B, Holden TM, Tomé CN, Varma R (2003) A neutron diffraction and modeling study of uniaxial deformation in polycrystalline beryllium. Metall Mater Trans 34A: 1439-1449

Bunge H-J (1965) Zur Darstellung allgemeiner Texturen. Z Metallk 56:872-874

Bunge H-J (1982) Texture Analysis in Materials Science – Mathematical Methods. Butterworths

Bunge H-J (1989) Texture and magnetic properties. Textures Microstructures 11:75-91

Bunge H-J, Wenk H-R, Pannetier J (1982) Neutron diffraction texture analysis using a position sensitive detector. Textures Microstructures 5:153-170

Dahms M, Bunge H-J (1988) A positivity method for the determination of complete orientation distribution functions. Textures Microstructures 10:21-35

Darling TW, TenCate JA, Brown DW, Clausen B, Vogel SC (2004) Neutron diffraction study of the contribution of grain contacts to nonlinear stress-strain behavior. Geophys Res Lett 31, doi:10.1029/2004GL020463

Daymond MR (2006) Internal stresses in deformed crystalline aggregates. Rev Mineral Geochem 63:427-458

DeWall H, Bestmann M, Ullemeyer K (2000) Anisotropy of diamagnetic susceptibility in Thassos marble: a comparison between measured and modeled data. J Struct Geol 22:1761-1771

Dornbusch HJ, Skrotzki W, Weber K (1994) Development of microstructure and texture in high-temperature mylonites from the Ivrea Zone. *In*: Textures of Geological Materials. Bunge HJ et al. (Eds) Deutsch. Gesell. Metallkunde, p 187-202

Feldmann K (1989) Texture investigation by neutron time-of-flight diffraction. Textures Microstructures 10: 309-323

Gastreich M, Jansen E, Raith M, Kirfel A (2000) Polfigurmessungen mit Neutronen an einem Orthopyroxen-Sillimanit-Granulit. Z Kristall (Suppl.) 17: 73

Ghildiyal H, Jansen E, Kirfel A (1999) Volume texture of a deformed quartzite observed with U-stage and neutron diffractometery. Textures Microstructures 31:239-248

Günther A, Brokmeier H-G, Petrovsky E, Siemes H, Helming K, Quade H (2002) Mineral preferred orientation and magnetic properties as indicators of varying strain conditions in naturally deformed iron ore. Appl Phys A 74:1080-1082

Hansen A, Chadima M, Cifelli F, Brokmeier H-G, Siemes H (2004) Neutron pole figures compared with magnetic preferred orientations of different rock types. Physica B 350:120-122

Harrison RJ (2006) Neutron diffraction of magnetic materials. Rev Mineral Geochem 63:113-143

Helming K, Schmidt D, Ullemeyer K (1996) Preferred orientations of mica bearing rocks described by texture components. Textures Microstructures 25:211-222

Henning K, Wieser E, Betzl M, Feldmann K (1981) Magnetic texture (Magnetic pole figures). Proceedings of the 6th International Conference on Texture of Materials, Tokyo, Japan (The Iron and Steel Institute of Japan) Vol. 2:967

Höfler S, Will G, Hamm H-M (1988) Neutron diffraction pole figure measurements on iron meteorites. Earth Planet Sci Lett 90:1-10

Ivankina TI, Kern H, Nikitin AN (2005) Directional dependence of P- and S- wave propagation and polarization in foliated rocks from the Kola superdeep well: Evidence from laboratory measurements and calculations based on TOF neutron diffraction. Tectonophysics 407:25-42

Jansen EM, Brokmeier H-G Siemes H (1996) Neutron texture investigations on natural Mt. Isa chalcopyrite ore. Part II: Preferred orientation of chalcopyrite after different experimental deformation conditions. Textures Microstructures 28: 1-15

Jansen EM, Brokmeier H-G, Siemes H (1996) Neutron texture investigations on natural Mt.Isa chalcopyrite ore. Part I: Preferred orientation of one and the same chalcopyrite sample before and after experimental deformation. Textures Microstructures 26:167-179

Jansen EM, Merz P, Schaeben H, Schäfer W, Siemes H, Will G (1992) Determination of preferred orientation of pyrite in a chalcopyrite ore by means of neutron diffraction. Textures Microstructures 19:203-210

Jansen EM, Siemes H, Merz P, Schäfer W, Will G, Dahms M (1993) Preferred orientation of experimentally deformed Mt. Isa chalcopyrite ore. Mineral Mag 57:45-53

Juul Jensen DJ, Leffers T (1989) Fast texture measurements using position sensitive detector. Textures Microstructures 10:361-374

Kallend JS (2000) Determination of the orientation distribution from pole figure data. *In:* Texture and Anisotropy. Kocks UF, Tomé CN, Wenk H-R (eds) Cambridge University Press, p 102-125

Kallend JS, Kocks UF, Rollett AD Wenk H-R (1991) Operational texture analysis. Mater Sci Eng A132:1-11

Karato S-Y, Wenk H-R (eds) (2002) Plastic Deformation of Minerals and Rocks. Reviews in Mineralogy and Geochemistry, Volume 51. Mineralogical Society of America

Kocks U F, Tomé CN, Wenk H-R (2000) Texture and Anisotropy. Preferred Orientations in Polycrystals and Their Effect on Materials Properties, 2nd Paperback Edtn. Cambridge University Press

Kuhs WF, Hansen TC (2006) Time-resolved neutron diffraction studies with emphasis on water ices and gas hydrates. Rev Mineral Geochem 63: 171-204

Kunze K, Adams BL, Heidelbach F, Wenk H-R (1994) Local microstructural investigations in recrystallized quartzite using orientation imaging microscopy. Proc. ICOTOM 10, Mater Sci Forum 157-162:1243-1250

Kurz W, Jansen E, Hundenborn R, Pleuger J, Unzog W (2004) Microstructures and preferred orientations of omphacite in Alpine eclogites: implications for the exhumation of (ultra-) high pressure units. J Geodynamics 37:1-55

Larson AC, Von Dreele RB (2004) General Structure Analysis System (GSAS). Los Alamos National Laboratory Report LAUR 86-748

Leiss B, Gröger HR, Ullemeyer K, Lebit H (2002)Textures and microstructures of naturally deformed amphibolites from the northern Cascades, NW USA. *In:* Deformation Mechanisms, Rheology and Tectonics: Current Status and Future Perspectives. De Meer S, Drury MR, De Bresser JHP, Pennock GM (eds) Geological Society, London, Special Publications, 200:219-238

Leiss B, Molli G (2003) "High-Temperature" texture in naturally deformed calcite marble from the Alpi Apuane, Italy. J Struct Geol 25:649-658

Leiss B, Siegesmund S, Weber K (1999): Texture asymmetries as shear sense indicators in naturally deformed mono- and polyphase carbonates. Textures Microstructures 33:61-74

Leiss B, Weiss T (2000) Fabric anisotropy and its influence on physical weathering of different types of Carrara marbles. J Struct Geol 22:1737-1745

Lloyd GE, Schmidt N-H, Mainprice D, Prior DJ (1991) Crystallographic textures. Mineral Mag 55:331-345

Lonardelli I, Wenk H-R, Lutterotti L, Goodwin M (2005) Texture analysis from synchrotron diffraction images with the Rietveld method: dinosaur tendon and salmon scale. J Synchr Radiation 12: 354-360

Lutterotti L, Matthies S, Wenk H-R, Schultz AJ, Richardson J W (1997) Combined texture and structure analysis of deformed limestone from time-of-flight neutron diffraction spectra. J Appl Phys 81:594-600

Matthies S (1979) On the reproducibility of the orientation distribution function of texture samples from pole figures (ghost phenomena). Phys Stat Sol (b) 92:K135-138

Matthies S, Pehl J, Wenk H-R, Lutterotti L, Vogel S (2005) Quantitative texture analysis with the HIPPO TOF diffractometer. J Appl Cryst 38:462-475

Matthies S, Vinel GW (1982) On the reproduction of the orientation distribution function of textured samples from reduced pole figures using the concept of conditional ghost correction. Phys Stat Sol (b) 112:K111-114

Merz P, Jansen E, Schaefer E, Will G (1990) PROFAN-PC: a PC program for powder peak profile analysis. J Appl Cryst 23:444-445

Monteiro PJM, Shomglin K, Wenk H-R, Hasparyk NP (2001) Effect of aggregate deformation on alkali-silica reaction. ACI Materials J 98:179-183

Morris PR (1959) Reducing the effects of nonuniform pole distribution in inverse pole figure studies. J Appl Phys 30:595-596

Niederschlag E, Siemes H (1996) Influence of initial texture, temperature and total strain on the texture development of polycrystalline pyrrhotite ores in deformation experiments. Textures Microstructures 28:129-148

Parise JB (2006) Introduction to neutron properties and applications. Rev Mineral Geochem 63:1-25

Pehl J, Wenk H-R (2005) Evidence for regional Dauphiné twinning in quartz from the Santa Rosa mylonite zone in Southern California. A neutron diffraction study. J Struct Geol 27:1741-1749

Pleuger J, Froitzheim N, Jansen E (2005) Folded continental and oceanic nappes on the southern side of Monte Rosa (western Alps, Italy): Anatomy of a double collision suture. Tectonics 24, TC4013, doi.1029/2004TC001737

Popa NC, Balzar D (2001) Elastic strain and stress determination by Rietveld refinement: Generalization treatment for textured polycrystals for all Laue classes. J Appl Cryst 34:187-195

Rajmohan N, Hayakawa Y, Szpunar JA, Root JH (1997) Neutron diffraction for stored energy measurement in interstitial free steel. Acta Mater 45:2485-2494

Randle V, Engler O (2000) Introduction to Texture Analysis: Macrotexture, Microtexture and Orientation Mapping. Gordon and Breach Science Publishers

Ratschbacher L, Wetzl A, Brokmeier H-G (1994) A neutron goniometer study of the preferred orientation of calcite in fine-grained deep-sea carbonate. Sedimentary Geol 89:315-324

Rietveld HM (1969) A profile refinement method for nuclear and magnetic structures. J Appl Cryst 2:65-71

Rosière CA, Siemes H, Quade H., Brokmeier H-G, Jansen EM (2001) Microstructures, textures and deformation mechanisms in hematite. J Structural Geol 23:1429-1440

Sander B (1950) Einführung in die Gefügekunde der Geologischen Körper, Vol. 2. Springer

Santisteban JR , Edwards L, Stelmukh V (2006), Characterization of textured materials by TOF transmission. Physica B (in press)

Schäfer W (2002) Neutron diffraction applied to geological texture and residual stress analysis. Eur J Mineral 14:263-290

Schmidt W (1925) Gefügestatistik. Tschermaks Mineral Petrograph Mitt 38:392-423

Schofield PF, Covey-Crump SJ, Stretton IC, Daymond MR, Knight KS, Holloway RF (2003) Using neutron diffraction measurements to characterize the mechanical properties of polymineralic rocks. Mineral Mag 67:967-987

Schwarzer RA, Weiland H (1988) Texture analysis by the measurement of individual grain orientations.-Electron microscopical methods and application to dual phase steel. Textures Microstructures 8-9: 443-456

Siegesmund S, Helming K, Kruse R (1994), Complete texture analysis of a deformed amphibolite: comparison between neutron diffraction and U-stage data. J Struct Geol 16:131-142

Siegesmund S, Ullemeyer K, Weiss T, Tschegg EK (2000) Physical weathering of marbles caused by anisotropic thermal expansion. Int J Earth Sci 89:170-182

Siemes H, Klingenberg B, Rybacki E, Naumann M, Schaefer W, Jansen E, Rosiere CA (2003) Texture, microstructure and strength of hematite ores experimentally deformed in the temperature range 600 °C to 1100 °C and at strain rates between 10^{-4} and 10^{-6} s^{-1}. J Struct Geol 25:1372-1391

Siemes H, Zilles D, Cox SF, Merz P, Schaefer W, Will G, Schaeben H, Kunze K (1993) Preferred orientation of experimentally deformed pyrite measured by means of neutron diffraction. Mineral Mag 57: 29-43

Skrotzki W, Helming K, Brokmeier H-G, Dornbusch H-J, Welch P (1995) Textures in pure shear deformed rock salt. Textures Microstruct 24:133-141

Skrotzki W, Tamm R, Oertel C-G, Röseberg J, Brokmeier H-G (2000) Microstructure and texture formation in extruded lead sulfide. J Struct Geol 22:1621-1632

Ullemeyer K, Helming K, Siegesmund S (1994) Quantitative texture analysis of plagioclase. *In:* Textures of Geological Materials. Bunge HJ, Siegesmund S, Skrotzki W, Weber K (eds) DMG Informationsgesells chaft, p 93-108

Ullemeyer K, Siegesmund S, Rasolofosaon PNJ, Behrmann JH (2006) Experimental and texture-derived P-wave anisotropy from the TRANSALP traverse: An aid for the interpretation of seismic field data. Tectonophysics 414: 97-116

Ullemeyer K, Spalthoff P, Heinitz J, Isakov NN, Nikitin AN, Weber, K (1998) The SKAT texture diffractometer at the pulsed reactor IBR-2 at Dubna: experimental layout and first measurements. Nucl Instrum Methods A 412:80-88

Ullemeyer K, Weber K (1999) Lattice preferred orientation as an indicator of a complex deformation history of rocks. Textures Microstructures 33:45-60

Van Houtte P (1991) A method for the generation of various ghost correction algorithms – the example of the positivity method and the exponential method. Textures Microstructures 13:199-212

Vogel SC, Priesmeyer H-G (2006) Neutron production, neutron facilities and neutron instrumentation. Rev Mineral Geochem 63:27-57

Von Dreele RB (1997) Quantitative texture analysis by Rietveld refinement. J Appl Cryst 30:517-525

Wahlstrom EE (1979) Optical Crystallography. Wiley

Walther K, Ullemeyer K, Heinitz J, Betzl M, Wenk H-R (1995) TOF texture analysis of limestone standard: Dubna results. J Appl Cryst 28: 503-507

Wang YD, Peng RL, Wang X-L, McGreevy RL (2002) Grain-orientation-dependent residual stress and the effect of annealing in cold-rolled stainless steel. Acta Mater 50:1717-1734
Wang YD, Wang X-L, Stoica AD, Richardson JW, Lin Peng R (2003) Determination of the stress orientation distribution function using pulsed neutron sources. J Appl Cryst 36:14-22
Wenk H-R (1985) Preferred Orientation in Deformed Metals and Rocks: An Introduction to Modern Texture Analysis. edited by H. R. Wenk, pp. 11-47, Academic Press
Wenk H-R (1991) Standard project for pole figure determination by neutron diffraction. J Appl Crystallogr 24: 920-927
Wenk H-R (1994) Texture analysis with TOF neutrons. In: Time-of-Flight Diffraction at Pulsed Neutron Sources (JD Jorgensen and AJ Schultz. Edts.), Trans Am Cryst Assn 29: 95-108
Wenk HR (1999) A voyage through the deformed Earth with the self-consistent model. Model Simul Mater Sci Eng 7:699-722
Wenk H-R Grigull S (2003) Synchrotron texture analysis with area detectors. J Appl Crystallogr 36:1040-1049
Wenk H-R Lonardelli I, Vogel SC, Tullis J (2005) Dauphiné twinning as evidence for an impact origin of preferred orientation in quartzite: An example from Vredefort, South Africa. Geology 33:273-276
Wenk H-R Pehl J, Williams DJ (2002) Texture changes during the quartz α–β phase transition studied by neutron diffraction. Los Alamos National Laboratory report LA-14036-PR, 36-39
Wenk H-R, Bunge HJ, Jansen E, Pannetier J (1985) Preferred orientation of plagioclase - neutron diffraction and U-stage data. Tectonophysics 126:271-284
Wenk H-R, Cont L, Xie Y, Lutterotti L, Ratschbacher L, Richardson J (2001) Rietveld texture analysis of Dabie Shan eclogite from TOF neutron diffraction spectra. J Appl Crystallogr 34:442-453
Wenk H-R, Huensche I, Kestens L (2006b) *In situ* observation of texture changes in ultralow carbon steel. Mater Trans (in press)
Wenk H-R, Kern H, Schäfer W, Will G (1984) Comparison of x-ray and neutron diffraction in texture analysis of carbonate rocks. J Struct Geol 6:687-692
Wenk HR, Kocks UF (1987) The representation of orientation distributions. Metall Trans 18A:1083-1092
Wenk H-R, Larson AC, Vergamini PJ, Schultz AJ (1991) TOF of pulsed neutrons and 2d detectors for texture analysis of deformed polycrystals. J Appl Phys 70:2035-2040
Wenk H-R, Lonardelli I, Franz H, Nihei K, Nakagawa S (2006a) Texture analysis and elastic anisotropy of illite clay. Geophysics (in press)
Wenk H-R, Lonardelli I, Williams D (2004) Texture changes in the hcp-bcc-hcp transformation of zirconium studied *in situ* by neutron diffraction. Acta Mater 52:1899-1907
Wenk H-R, Lutterotti L, Vogel S (2003) Texture analysis with the new HIPPO TOF diffractometer. Nucl Instrum Methods A515:575-588
Wenk H-R, Matthies S, Donovan J, Chateigner D (1998) BEARTEX, a Windows-based program system for quantitative texture analysis. J Appl Cryst 31:262-269
Wenk H-R, Matthies S, Lutterotti L (1994) Texture analysis from diffraction spectra. *In:* Textures of Materials ICOTOM-10. Bunge HJ (ed) Switzerland: Trans. Tech. Pubs. 157-162:473-479
Wenk H-R, Pannetier J (1990) Texture development in deformed granodiorites from the Santa Rosa mylonite zone, southern California. J Struct Geol 12:177-184
Xie Y, Wenk H-R, Matthies S (2003) Plagioclase preferred orientation by TOF neutron diffraction and SEM-EBSD. Tectonophysics 370:269-286
Young RA (1993) The Rietveld Method. International Union of Crystallography, Oxford University Press
Zeisig A, Weiss T, Siegesmund S (2002) Thermal expansion and its control on the durability of marbles. *In:* Natural Stones, Weathering Phenomena, Conservation Strategies and Case Studies. Siegesmund S, Weiss T, Vollbrecht A (eds) Geological Society Special Publication 205:57-72
Zink U, Brokmeier H-G and Bunge HJ (1994) Determination of magnetic textures in ferromagnetics by means of neutron diffraction. Mater Sci Forum 157-162:251-256
Zink U, Bunge HJ, Brokmeier H-G (1997) Neutron texture measurement with applied magnetic field. Physica B 234-236:980-982